8. Inorganic Geochemical Characterization of Lithologic Units Recovered during ODP Leg 207 (Demerara Rise)[1]

Almut Hetzel,[2] Hans-Jürgen Brumsack,[2] Bernhard Schnetger,[2] and Michael E. Böttcher[3]

ABSTRACT

The Cretaceous and Paleogene sediments recovered during Ocean Drilling Program Leg 207 can be divided into three broad modes of deposition: synrift clastics (lithologic Unit V), organic matter–rich, laminated black shales (Unit IV), and open-marine chalk and calcareous claystones (Units III–I). The aim of this study is to provide a quantitative geochemical characterization of sediments representing these five lithologic units. For this work we used the residues (squeeze cakes) obtained from pore water sampling. Samples were analyzed for bulk parameters (total inorganic carbon, total organic carbon, and S) and by X-ray fluorescence for major (Si, Ti, Al, Fe, Mn, Mg, Ca, Na, K, and P) and selected minor (As, Ba, Co, Cr, Cu, Mo, Ni, Pb, Rb, Sr, U, V, Y, Zn, and Zr) elements. Inductively coupled plasma–mass spectrometry analyses for rare earth elements (REEs) were performed on acid digestions of the squeeze cake samples from Site 1258.

The major element composition is governed by the mixture of a terrigenous detrital component of roughly average shale (AS) composition with biogenous carbonate and silica. The composition of the terrigenous detritus is close to AS in Units II–IV. For Unit I, a more weathered terrigenous source is suggested. Carbonate contents reach >60 wt% on average in chalks and calcareous claystones of Units II–IV. The SiO_2 contribution in excess of the normal terrigenous-detrital background indicates the presence of biogenous silica, with highest amounts in Units II

and III. The contents of coarse-grained material (quartz) are enhanced in Unit V, where Ti and Zr contents are also high. This indicates a high-energy depositional environment. REE patterns are generally similar to AS. A more pronounced negative Ce anomaly in Unit IV may indicate low-oxygen conditions in the water column. The Cretaceous black shales of Unit IV are clearly enriched in redox-sensitive and stable sulfide-forming elements (Mo, V, Zn, and As). High phosphate contents point toward enhanced nutrient supply and high bioproductivity. Ba/Al ratios are rather high throughout Unit IV despite the absence of sulfate in the pore water, indicating elevated primary production. Manganese contents are extremely low for most of the interval studied. Such an Mn depletion is only possible in an environment where Mn was mobilized and transported into an expanded oxygen minimum zone ("open system"). The sulfur contents show a complete sulfidation of the reactive iron of Unit IV and a significant excess of sulfur relative to that of iron, which indicates that part of the sulfur was incorporated into organic matter. We suppose extreme paleoenvironmental conditions during black shale deposition: high bioproductivity like in recent coastal upwelling settings together with severe oxygen depletion if not presence of hydrogen sulfide in the water column.

INTRODUCTION

During Ocean Drilling Program (ODP) Leg 207, expanded, shallowly buried Cretaceous and Paleogene sediments from Demerara Rise off Suriname, South America, were recovered. This period of the Earth's history involved episodes of ocean anoxia, rapid climate change, mass extinction, and opening of the Equatorial Atlantic Gateway. Therefore, the Demerara Rise provides ideal conditions for long-term paleoceanographic studies of the tropical Atlantic (Erbacher, Mosher, Malone, et al., 2004).

Our approach is to use bulk sediment geochemical data to analyze the sedimentation history of Demerara Rise. Major element composition provides insight into the relative proportions of major components in marine sediment: terrigenous detritus, biogenous material, and diagenetic products. Elements and element ratios related to terrigenous material also help to identify provenance characteristics and thus changes in climate and/or sediment supply. Cross-correlation analysis of elements gives information about different mineral phases suggesting different depositional environmental features. Changes in paleoproductivity are mirrored by elements related to biogenous processes, and the oxygenation state of the water column may be deduced from the abundance of redox-sensitive elements. Beside these paleoceanographic studies, element distribution patterns in pore water reveal information about postdepositional and ongoing diagenesis in the sediment. Study of the whole sediment column can therefore help to locate the depth of past and still-active biogeochemical processes.

The aim of this study is to provide a quantitative geochemical characterization of sediments representing the five lithologic units encountered during Leg 207. For this work, we used the cakes obtained from pore water squeezing. The advantage of this material is its suitability for later chemical analysis in onshore laboratories. Another advantage is its lower content of pore water. Because the effects of precipitated dissolved seawater salts are reduced, no otherwise essential salt correction is applied. We show that the material is useful for providing a first over-

view of the lithologic units by applying standard geochemical analytical methods.

MATERIALS AND METHODS

Site Description

During Leg 207, sediments were recovered from five Sites (1257–1261) on Demerara Rise, located at ~9°N in the western tropical Atlantic (Fig. F1). The rise stretches ~380 km along the coast of Suriname and reaches a width of ~220 km from the shelf break to the northeastern escarpment, where water depths increase sharply from 1000 to >4500 m. Whereas most of the plateau lies in shallow water (700 m), the northwestern margin forms a gentle ramp reaching water depths of 3000–4000 m. Nearly uniform, shallowly buried sections of Cretaceous and Paleogene age were drilled with good stratigraphic control. The five drill sites (Sites 1257–1261) constitute a depth transect with water depths ranging from 1900 to 3200 m. The sediments recovered can be divided into three broad styles of deposition: synrift clastics (lithologic Unit V), organic matter–rich, laminated black shales (Unit IV), and open-marine chalk and calcareous claystones (Units III–I) (Erbacher, Mosher, Malone, et al., 2004).

On board, interstitial waters from 152 samples from Sites 1257–1261 and covering a depth range from the sediment/seawater interface to 648 meters composite depth were collected and processed using standard ODP methods. Interstitial water samples were squeezed from sediment samples immediately after retrieval of the cores using titanium squeezers, modified after the standard ODP stainless steel squeezer (Manheim and Sayles, 1974). On board the ship, splits of all squeeze cakes (pore water squeezing residues) were taken, freeze-dried, and stored in polyethylene bags. In the home laboratory, the squeeze cake samples were ground and homogenized in an agate ball mill. The powdered samples were used for all subsequent geochemical analyses. The classification of lithologic units follows the scheme given by Erbacher, Mosher, Malone, et al. (2004).

Carbon and Sulfur

Total sulfur (TS) and total carbon (TC) were analyzed using a LECO SC-444 infrared analyzer. Total inorganic carbon (TIC) was determined coulometrically using a UIC CM 5012 CO_2 coulometer coupled to a CM 5130 acidification module. Total organic carbon (TOC) was calculated as the difference between TC and TIC. For detailed information on precision and accuracy of the methods applied see Prakash Babu et al. (1999).

Major and Trace Elements

For X-ray fluorescence (XRF) analysis, 600 mg of sample was mixed with 3600 mg of a 1:1 mixture of dilithium tetraborate ($Li_2B_2O_7$) and lithium metaborate ($LiBO_2$), preoxidized at 500°C with NH_4NO_3, and fused into glass beads. The glass beads were analyzed by XRF (Philips PW 2400) calibrated with 29 carefully selected geostandards. Analytical precision was >2% for major elements (Si, Ti, Al, Fe, Mn, Mg, Ca, Na, K,
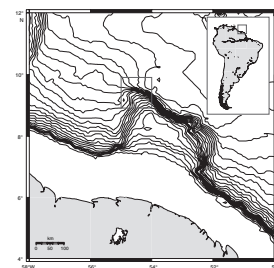
and P) and >6% for minor elements (As, Ba, Co, Cr, Cu, Mo, Ni, Rb, Sr, V, Y, Zn, and Zr), except for Pb and U (6%–10%).

Rare Earth Elements

Samples from Site 1258 were also analyzed by inductively coupled–plasma mass spectrometry (ICP-MS). For acid digestion, 50 mg of sample was preoxidized with 1 mL of HNO_3 (65%) in polytetrafluoroethylene (PTFE) vessels overnight and heated with 3 mL of HF (40%) and 3 mL of $HClO_4$ (70%) in closed PTFE autoclaves (PDS-6) for 6 hr at 180°C. The acids were then evaporated on hot plates at 180°C to incipient dryness. Afterward, 3 mL of 6-N HCl aliquots were added and evaporated at 180°C. This step was repeated three times. The wet precipitate was dissolved in 1 mL of HNO_3 (65%), diluted to ~10 mL, and simmered at 60°C for 1 hr. The acid digestions were brought up to 50 mL final volume with deionized water. Only acids purified by subboiling distillation (HNO_3, HCl, and $HClO_4$) or of suprapure (HF) quality were used. Rare earth element (REE) analyses were carried out using an Element (Finnigan MAT, Germany) high-resolution (HR)-ICP-MS. Analytical precision as checked by multiple analyses of international reference materials (see "Appendix," p. 14; Table AT1) is >7%.

RESULTS AND DISCUSSION

In a very simplistic way, Demerara Rise sediments consist of variable mixtures of terrigenous detritus (represented by Al_2O_3 and SiO_2) and biogenous material (represented by CaO and SiO_2). To compare the relative proportions of the major components, the relative proportions of CaO (mostly carbonate), SiO_2 (quartz/opal and alumosilicates), and Al_2O_3 (alumosilicates) are plotted in a triangle diagram (Fig. F2) (Brumsack, 1989). For comparison, average shale (AS) (Wedepohl, 1971), K-feldspar, and kaolinite are also plotted.

Sediments of lithologic Unit I (Fig. F2A) plot on a straight mixing line between carbonate and a clay component richer in Al than AS. This suggests that more intensely weathered clays (possibly a higher kaolinite proportion) are characteristic for Unit I sediments. Unit I samples show no additional enrichment in SiO_2, ruling out that significant amounts of biogenic silica are present. Given the present lack of quantitative mineral data, the presence of biogenic silica could be obscured if a higher proportion of kaolinite were present.

Most sediments of Units II–IV (Fig. F2B) plot on a mixing line of AS and carbonate but show varying contents of biogenic silica. Unit II sediments are particularly rich in carbonate, whereas Unit III samples are generally lower in carbonate. The shift toward the SiO_2 edge indicates higher excess silica contents.

Samples of Unit V (Fig. F2C) show a rather variable distribution. Excess silica contents are high in samples with low carbonate contents. This excess silica reflects the abundance of coarse-grained, quartz-rich sand in Unit V rather than to biogenous silica that typifies Units II–IV.

In Figure F3, we present an overview of the changing proportion of major components of all lithologic units. For calculations of major components listed in Table T1, we consider that

F2. Major components of sediments, p. 16.
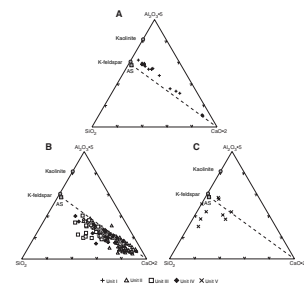
F3. Proportion of major components, p. 17.
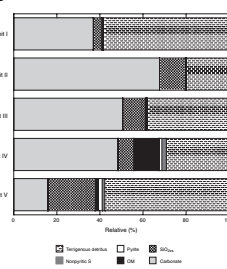
T1. Calculations of proportions of major components, p. 26.

1. Carbonate contents are calculated from ΣCO_2 (TIC), assuming all TIC is present as pure $CaCO_3$.
2. Excess SiO_2 (biogenous opal and/or quartz) is estimated by subtracting the amount of SiO_2 present in alumosilicates from total SiO_2. We assume that the minimum SiO_2/Al_2O_3 ratio of each individual unit serves as terrigenous background, unless only SiO_2/Al_2O_3 ratios higher than AS are encountered. In this case, the SiO_2/Al_2O_3 ratio of AS serves as the background value for calculating SiO_{2xs}.
3. Organic matter (OM) contents are calculated by multiplying TOC by a factor of 1.34, a value given by Tissot and Welte (1984) for Type II kerogen.
4. Based on the Fe to S stoichiometry of pyrite, its contents can either be calculated from TS values, assuming all TS is present as pyrite, or from Fe, assuming all Fe is present as pyrite. Because the latter is unlikely, pyrite contents based on TS values are used unless they overnumbered the pyrite content based on Fe. In this case the excess sulfur fraction represents the "nonpyritic S" component.
5. The fraction we term "terrigenous detritus" equals the difference between 100 wt% and the sum of major components calculated above. Comparing our assumed terrigenous detritus with the sum of terrigenous elements analyzed exhibits a very good correlation ($R^2 = 0.997$) (Fig. F4).

Sediments from Demerara Rise are dominated by either carbonate or terrigenous detritus (Fig. F3). For lithologic Unit I, the terrigenous detritus forms the major component (>58 wt%). The average carbonate content is 37.0 wt%. The SiO_{2xs} content (4.0 wt%) is the lowest found in any lithologic unit. Concentrations of OM and pyrite are <0.3 wt% and nonpyritic sulfur is absent in Unit I.

In Units II–III, carbonate (nannofossils, foraminifers, and partly diagenetic calcite) forms the major component, with concentrations that average 67.7 wt% in Unit II and 50.6 wt% in Unit III. SiO_{2xs} contents (siliceous microfossils, radiolarians, and zeolites) are ~11 wt% in these sediments. According to low quantities of OM (<0.3 wt%), pyrite (<0.4 wt%), and nonpyritic sulfur (absent in Unit II, <0.1 wt% in Unit III), 20.1 wt% in Unit II and 38.1 wt% in Unit III of the sediment are terrigenous detritus.

The laminated black shales of Unit IV (of Cenomanian–Santonian age) are characterized by high OM contents (mean value >12 wt%, up to 24.9 wt% for individual samples). The content of pyrite is comparably low (0.7 wt%) in comparison to the amount of nonpyritic sulfur (2.1 wt%). This indicates a significant Fe limitation during pyrite formation and the sulfidation of OM. Beside the dilution effect of these components, the relative proportions of carbonate (48.4 wt%), terrigenous detritus (29.2 wt%), and SiO_{2xs} (7.3 wt%) are similar to those found in overlying sediments of Unit III.

Like Unit I, Unit V is dominated by terrigenous detritus (57 wt%). The average carbonate concentrations (15.9 wt%) are the lowest found in lithologic units of Demerara Rise. In sediments of Unit V, siliceous microfossils are rare. Their former presence is indicated by zeolites. However, high amounts of SiO_{2xs} (21.9 wt%) are mostly due to quartz, which is in accordance with the presumed shallow synrift deposit (Erbacher, Mosher, Malone, et al., 2004) (see discussion below). OM and

F4. Correlation of two calculation methods for terrigenous detritus, p. 18.
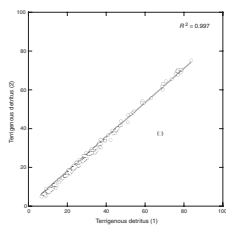
pyrite contents are each 1.6 wt%. Thus, the pyrite content is highest in Unit V, whereas nonpyritic sulfur is present in smaller quantities (1.3 wt%) than in Unit IV.

The chemical index of alteration (CIA) (Taylor and McLennan, 1985) is a well-established parameter for determining the degree of weathering. During the degradation of feldspars, Ca, Na, and K are removed and clay minerals with a higher fraction of Al are formed. The CIA is estimated from the proportion of Al_2O_3 vs. the weathering-prone oxides:

$$CIA = [Al_2O_3/(Al_2O_3 + CaO^* + Na_2O + K_2O)] \times 100,$$

where CaO* represents the amount of CaO incorporated in the silicate fraction. A correction for carbonate and apatite content is therefore necessary. Unaltered feldspars have a CIA of 50, whereas kaolinite has a value of 100 (total removal of alkali elements). We understand that CIA values in carbonate-rich sediments may lead to compromised results. The correction required for carbonate often leads to negative CaO* values because of the presence of additional carbonate phases like dolomite. In this case, CaO* contents were assumed to be zero. This may lead to an overestimation of CIA values due to an underestimation of CaO*.

As described above and shown in Figure F3 and Table T1, we assumed that the terrigenous detritus round off the major components we calculated from the chemical analyses to 100 wt%. When dividing the terrigenous detritus component of each sample by the Al_2O_3 content, a factor f is obtained, which represents the relative abundance of Al_2O_3 in this component. The reciprocal value of this factor $1/f$ (= weathering factor [WF]) should be a parameter for the degree of weathering, comparable to the CIA, but based on a broader range of chemical compounds.

In Figure F5 we compare WF with CIA values calculated for the lithologic units. Standard deviations (1σ) and results for AS (Wedepohl, 1971) are shown as well.

Both parameters require a number of simplifications and assumptions and therefore bear uncertainties. The values of the CIA as well as WF spread within the different lithologic units. The standard deviations (<13 rel%) overlap for both parameters. Only qualitative interpretations of the mean values for each unit are possible. Nevertheless, the weak correlation between both parameters ($R^2 = 0.55$) indicates that differences in weathering intensity did occur, since we can easily distinguish Units II–IV from Units I and V regarding their state of weathering.

For Units II, III, and IV, values for both parameters, CIA as well as WF, are essentially the same as for AS (CIA = 70–75) (Taylor and McLennan, 1985) and thus support our interpretation of Figure F2, where a terrigenous component similar in composition to AS is assumed.

The terrigenous material from Unit I is characterized by a CIA > 80, indicating a high degree of weathering. Taylor and McLennan (1985) report CIA values between 80 and 90 for the Amazon mud cone. This is confirmed by the WF. Deposition of lithologic Unit I began in the middle Miocene (Erbacher, Mosher, Malone, et al., 2004), which coincides with the initial uplift of the Andes. Resulting changes in provenance and/or drainage pathways (Potter, 1997) may have led to different characteristics of the terrigenous detritus in Unit I, in agreement with our observations from Figure F2.

In Unit V, where only one sample was encountered with CaO* contents >0 wt%, it is suggested that the CaO* content is underestimated

F5. Comparison of WF and CIA values, p. 19.
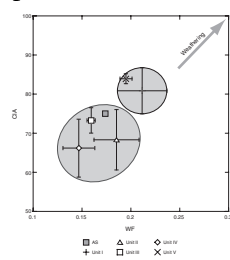
and therefore the high CIA value is incorrect. WF indicates more intense weathering, but a clear conclusion cannot be drawn for such quartz-rich sediments.

In Figure F6, the concentrations of TiO_2 (Fig. F6A) and Zr (Fig. F6B) are plotted vs. Al_2O_3. To avoid simple dilution effects when crosscorrelating element abundances, all samples were calculated on a "carbonate-free" basis. This calculation is based on the assumption that all TIC is present as pure $CaCO_3$, which may lead to an underestimation for Ca and an overestimation for other carbonate-forming cations (mainly Mg and Sr, see discussion below). The resulting carbonate-free sediment still contains biogenous Si.

Data points from Units I–IV plot on a line (R^2 = 0.93 for TiO_2 and R^2 = 0.65 for Zr), indicating that TiO_2 and Zr are more or less uniformly incorporated into the clay component of these units. The observation that the AS data plot above the correlation line supports our interpretation that the terrigenous detrital component in Units I–IV is enriched in Al, possibly because of more intense weathering. Samples from Unit V plot above this line and show a negative correlation with Al_2O_3 (R^2 = 0.74 for TiO_2 and R^2 = 0.86 for Zr). We conclude that an additional TiO_2- and Zr-bearing component other than clay minerals must be present in Unit V, most likely heavy minerals in the coarser-grained sands. In Figure F6C and F6D, the concentrations of TiO_2 and Zr are plotted vs. SiO_{2xs} (calculation as above but using carbonate-free data). Samples from Units I–IV again plot on a line (R^2 = 0.53 for TiO_2 and R^2 = 0.33 for Zr). The negative correlation shows that SiO_{2xs} behaves independently of the terrigenous-detrital component and is generally higher in samples with lower clay content. The same is essentially true for SiO_{2xs} and Zr. By contrast, for samples from Unit V, a positive correlation is observed between SiO_{2xs} and Zr (R^2 = 0.86) or TiO_2 (R^2 = 0.82). We assume that the SiO_{2xs} from Units I–IV is derived from biogenous Si, which serves as a diluent for the terrigenous component in the carbonate-free sediment, whereas TiO_2 and Zr contents are higher in the quartz-rich sands of Unit V. Elevated quartz and heavy mineral abundances signify high-energy environments (Dellwig et al., 2000), supporting the idea that Unit V sediments are of synrift origin as stated by Erbacher, Mosher, Malone, et al. (2004).

The REEs are regarded as being almost insoluble and are present in only very low concentrations in seawater and river water (McLennan, 1989). Thus, the REEs present in sediments are mainly transported as particulate matter. Because the effects of diagenesis are minor, REEs reflect the chemistry of their source areas and can be used for provenance studies. Sedimentary sorting can affect the concentrations of REE: clays show higher abundances than do coarser-grained sediments. The relative composition of REEs are generally similar for sandstones and shales. Quartz has only a diluting effect. The presence of heavy minerals may have an effect on the REE composition of an individual sample; however, a large heavy mineral contribution would be required to significantly change distribution patterns. The REE compositions of biogenous carbonates and chemical sediments in general reflect the REE composition of the surrounding seawater (McLennan, 1989). But again, high quantities are necessary to cause changes in the REE character of the sediment relative to the primary detrital flux. The REEs have generally similar chemical and physical properties. This arises from the fact that they all form stable 3+ ions of similar size. A small number of the

F6. Scatter plots for heavy minerals, p. 20.
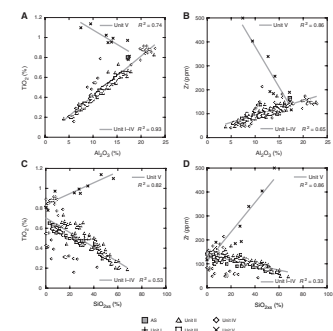
REEs also exist in oxidation states other than 3+, but the only ions of geological importance are Ce^{4+} and Eu^{2+}. Changes in redox conditions can therefore affect the chemistry and thus the solubility of these two elements and lead to enrichments or deficiencies relative to other REEs. In a normalized REE distribution pattern, a positive or negative "anomaly" would result.

The average REE distribution patterns for the individual units are shown in Figure F7. To avoid dilution because of high carbonate contents, element/Al ratios are used. Elemental ratios are normalized to element/Al ratios of upper continental crust (Taylor and McLennan, 1985). Values between 1 and 2 for sediments of Units I–IV indicate a weak REE enrichment, whereas sediments of Unit V show a small depletion in REEs (values between 0.7 and 1). A slightly more pronounced negative Ce anomaly is seen in Unit IV relative to the other units. This Ce anomaly may be quantified by comparing the measured concentration (Ce) with an expected concentration (Ce*) obtained by interpolating between the values of the neighboring elements.

Wilde et al. (1996) linked Ce anomalies in shales of the anoxic facies to eustatic sea level changes. Similar to Mn, Ce^{4+} is less soluble under oxic conditions, whereas under anoxic conditions it will be mobilized, leading to a depletion in Ce in anoxic sediments relative to those deposited under oxic conditions. A negative Ce anomaly would result.

In Table T2, two different values are given for the Ce anomaly, which are based on different calculations. Taylor and McLennan (1985) recommended use of the geometric mean:

$$Ce^* = (La \times Pr)^{1/2}.$$

The ratio Ce/Ce* is then a measure of the anomaly, with values less than unity being termed negative. Wilde et al. (1996) support use of the arithmetic mean:

$$Ce^* = (La + Pr)/2$$

and calculated the logarithm of the ratio Ce/Ce*. Both calculations lead to essentially the same values for Ce*, with the most negative anomaly in Unit IV.

According to Wilde et al. (1996), the negative Ce anomaly for the black shales of Unit IV can be interpreted as a consequence of water column anoxia during sea level highstands in the Cretaceous. REE patterns in the sediments of Demerara Rise are complicated by the presence of biogenous and chemical compounds that record the surrounding seawater and pore water (e.g., for phosphate). For example, carbonate tests of plankton living in the photic zone under oxic conditions would carry the surface seawater characteristics and would therefore display a negative Ce anomaly. However, this effect is not seen in the more carbonate rich Units II and III.

The database is still too small for demonstrating that these REE characteristics hold true for Cenomanian/Turonian (C/T) black shales from Demerara Rise in general. Statistically, the REE patterns do not show any extraordinary characteristics and do not differ much from those of Post-Archean average Australian Shale (Taylor and McLennan, 1985).

Figure F8 illustrates the chemistry of the biogenous carbonates. In Figure F8A, CaO concentration is plotted vs. the TIC contents. The good correlation shows that almost all CaO is present as $CaCO_3$. Some

F7. Average REE distribution patterns, p. 21.
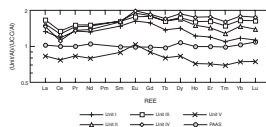
T2. Ce anomaly for lithologic Units I–V, p. 27.

F8. Scatter plots of carbonate chemistry, p. 22.
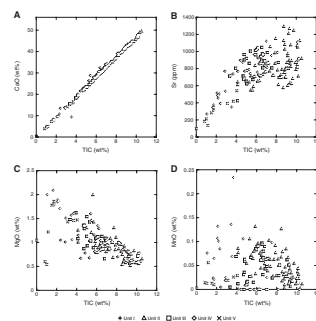
samples from Unit IV contain additional CaO, which is present as apatite. The contents of CaO-bearing mineral phases other than carbonate are negligible. The positive correlation between Sr and TIC (Fig. F8B) indicates that a variable fraction of Sr is incorporated into carbonates (750–1300 ppm). The negative correlation of MgO and TIC (Fig. F8C) shows that Mg is mostly incorporated into clay components, even though a small contribution of Mg-rich calcite or dolomite cannot be excluded. MnO shows no correlation with TIC (Fig. F8D), but highest concentrations of MnO are found in carbonate-rich Unit II. Figure F9 shows the average element/Al ratios of Ca, Sr, Mg, and Mn in Units I–V. Except for the strong Mn depletion in Unit IV (see discussion below), a similar distribution pattern is displayed.

The oxygenation state of the seawater and the redox state of the surface sediment form a crucial variable for the preservation of organic material and the formation of pyrite. Therefore, the contents of pyrite, reactive Fe, and TOC allow us to draw conclusions about the paleoenvironment during deposition of the sediment. The degree of pyritization based on bulk sediment analysis is visualized in a ternary Fe_x-TOC-S diagram (Fig. F10) (Brumsack et al., 1995). The content of reactive Fe (Fe_x) was estimated empirically ($Fe_x = Fe - 0.25 \times Al$) assuming that a certain fraction of alumosilicate-bound Fe is not available for pyrite formation (Canfield et al., 1992). Results of a detailed analysis of reactive iron in the investigated samples is discussed in an accompanying publication (Böttcher et al., this volume). Data points that plot close to the pyrite saturation line (PSL) are assumed to represent samples that are completely pyritized. Most of the samples of Unit IV plot below the PSL, indicating the presence of an additional sulfur phase. Böttcher et al. (this volume) found organic sulfur contents exceeding 3 wt% in Demerara Rise black shales. The presence of acid volatile sulfur points to the presence of metal sulfides other than pyrite, likely ZnS (Brumsack, 1980). Samples of Units I–III are positioned above the PSL, indicating that Fe_x was only partly used for pyrite formation, in agreement with direct measurements of sulfur and iron speciation (Böttcher et al., this volume).

Trace metal (TM) distribution patterns reveal information about the depositional environment. Because of TM participation in biocycling processes (Bruland, 1983), scavenging by particulate matter and dissolution and precipitation of redox-sensitive compounds TM enrichment as well as depletion in sediments are diagnostic for bioproductivity and redox conditions during deposition. In combination with pore water data, they allow indication of postdepositional element migration. Figure F11 shows the mean values of TM/Al ratios of diagnostic TM in the different lithologic units. TMs are shown in order of TM enrichment relative to AS (dashed line) in Unit IV.

The nonlithologenic excess Ba has been interpreted as a paleoproxy for bioproductivity (Schmitz, 1987; Dymond et al., 1992; Paytan et al., 1996). These biogenic barites ($BaSO_4$) (Bishop, 1988; Bertram and Cowen, 1997; Bernstein and Byrne, 2004) are only stable under seawater sulfate concentrations (Church and Wolgemuth, 1972). Because of the microbial sulfate reduction in TOC-rich sediments, barite is dissolved, Ba is mobilized (Brumsack and Gieskes, 1983; McManus et al., 1998; Eagle et al., 2003), and authigenic barite precipitates at the top of the sulfate-depletion zone forming diagenetic barite fronts within or above TOC-rich strata (Torres et al., 1996; Bréhéret and Brumsack, 2000).

F9. Mean values of element/Al ratios, p. 23.
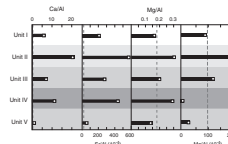
F10. Degree of pyritization of sediments, p. 24.
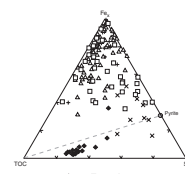
F11. Mean values of TM/Al ratios, p. 25.
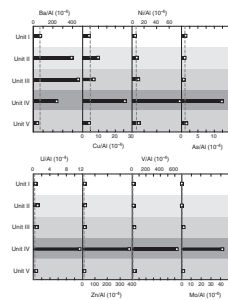
Ba/Al ratios are highest in Units II and III. In the black shales of Unit IV, Ba/Al ratios are still high despite the absence of sulfate in the pore water (Erbacher, Mosher, Malone, et al., 2004). Arndt et al. (2006) show in a transport-reaction model that not only OM degradation but also anaerobic oxidation of methane above the black shales of Demerara Rise influence sulfate availability and therefore the remobilization of biogenic barium. The authors further showed that temporal dynamics of degradation processes caused various shifts of the barite precipitation zone during burial, thus inhibiting the formation of an authigenic barite front or causing the dissolution of earlier formed fronts. In our view, the Ba enrichment in Unit IV indicates elevated primary productivity during deposition. But a large fraction of former barite may remobilize and form diagenetic barites in Unit III. For this reason, the use of Ba as a paleoproxy on a quantitative level (Dymond et al., 1992) for Cretaceous settings in such an environment is highly questionable.

The very high phosphate contents (>0.7 wt% P_2O_5 on average in Unit IV) are comparable to those in recent upwelling sediments and also points toward enhanced nutrient supply and resulting high bioproductivity (e.g., Böning et al., 2004).

The black shales of Unit IV are clearly enriched in redox-sensitive and stable sulfide–forming TMs. In today's ocean, TOC-rich sediments are deposited in coastal upwelling areas and euxinic basins. Brumsack (2006) attempted to distinguish both environments by their specific TM patterns. Thereby, the author discussed TM sources and fixation mechanisms. Cu and Ni are discussed to be involved in biocycling. The enrichment found in recent upwelling sediments (Böning et al., 2004) indicates deposition via biodetritus. In contrast, oxyanions (As, U, V, and Mo) are primarily derived from seawater. The enrichments of Mo, U, and As indicate a sulfidic environment (Brumsack, 2006). High concentrations of sulfide-forming TM (Cu and Zn) and sulfur phases other than pyrite indicate Fe limitation and thus support the idea of an euxinic environment (**Böttcher et al.,** this volume).

The strong depletion in Mn (Fig. **F9**) requires the presence of at least suboxic conditions in parts of the water column (Quinby-Hunt and Wilde, 1994). Dissolved Mn is conveyed away in an expanded oxygen minimum zone (OMZ) like in recent coastal upwelling areas. Thurow et al. (1992) describe such an Mn mobilization at the northwest Australian margin during the C/T boundary event. The authors found Mn-poor sediments within the OMZ and Mn-rich sediments below the OMZ, indicating oxic deep waters during the C/T interval at this location. Mn enrichment under anoxic/euxinic conditions is only possible in a closed (silled basin like) system, where dissolved Mn cannot be conveyed away and alkalinity is high enough to form Mn(II) carbonate. T.W. Lyons (pers. comm., 2006) finds these Mn-enrichments in euxinic Unit 1 in the modern Black Sea. Mn depletion in all samples of Unit IV shows that the investigated sites (Sites 1257–1261) must be located within the OMZ during deposition. In this case, the reoxidation and reduction of Mn oxides (Mn cycling) at the redox boundary may have induced TM scavenging by Mn (oxy)hydroxides (Cu, Mo, and V) comparable to the Black Sea. But the Mn most likely was deposited in other parts of the proto-Atlantic, where deep waters still might have contained oxygen.

However, one should mention that the elemental pattern of black shales from Demerara Rise is very similar to the one known from other C/T settings, particularly with respect to the extraordinarily high V and Zn contents (Brumsack, 2006).

CONCLUSIONS

Sediments recovered during Leg 207 from the Demerara Rise consist of different mixtures between biogenous carbonate and detrital material. Lithologic Units II–IV show high carbonate contents, whereas Unit I and V are dominated by terrigenous detritus. Major element analysis indicates a common origin of the terrigenous detritus similar to AS, whereas the clay-dominated Unit I reveals a more weathered terrigenous component. Heavy mineral phases and quartz-bearing sands display a high-energy synrift deposit in Unit V.

The Cretaceous black shales of Unit IV are clearly enriched in redox-sensitive and stable sulfide–forming elements. This indicates high paleo-productivity and severe oxygen depletion in the water column. The complete sulfidation of the black shales and significant excess sulfur report a sulfidic environment, leading to sulfur incorporation into organic matter.

Ba enrichments in sediments above the black shale sequences show former diagenetic mobilization of barite in underlying sediment layers. Pore water data evidence that sulfate reduction due to anaerobic methane oxidation is still driving barite diagenesis.

ACKNOWLEDGMENTS

REFERENCES

Arndt, S., Brumsack, H.-J., Hetzel, A., and Wirtz, K.W., 2006. Cretaceous black shales as active bioreactors: a biogeochemical model for the deep biosphere encountered during ODP Leg 207 (Demerara Rise). *Geochim. Cosmochim. Acta,* 70(2):408–425. **doi:10.1016/j.gca.2005.09.010**

Bernstein, R.E., and Byrne, R.H., 2004. Acantharians and marine barite. *Mar. Chem.,* 86(1–2):45–50. **doi:10.1016/j.marchem.2003.12.003**

Bertram, M.A., and Cowen, J.P., 1997. Morphological and compositional evidence for biotic precipitation of marine barite. *J. Mar. Res.,* 55(3):577–593. **doi:10.1357/0022240973224292**

Bishop, J.K.B., 1988. The barite-opal-organic carbon association in oceanic particulate matter. *Nature (London, U. K.),* 332:341–343. **doi:10.1038/332341a0**

Böttcher, P., Brumsack, H.-J., Bottcher, M.E., Schnetger, B., Kriete, C., Kallmeyer, J., and Borchers, S.L., 2004. Geochemistry of Peruvian near-surface sediments. *Geochim. Cosmochim. Acta,* 68(21):4429–4451. **doi:10.1016/j.gca.2004.04.027**

Bréhéret, J.G., and Brumsack, H.-J., 2000. Barite concretions as evidence of pauses in sedimentation in the Marnes Bleues Formation of the Vocontian Basin (SE France). *Sediment. Geol.,* 130(3–4):205–228. **doi:10.1016/S0037-0738(99)00112-8**

Bruland, K.W., 1983. Trace elements in seawater. *In* Riley, J.P., and Chester, R. (Eds.), *Chemical Oceanography* (Vol. 8): London (Academic Press), 157–220.

Brumsack, H.-J., 1980. Geochemistry of Cretaceous black shales from the Atlantic Ocean (DSDP Legs 11, 14, 36 and 41). *Chem. Geol.,* 31:1–25. **doi:10.1016/0009-2541(80)90064-9**

Brumsack, H.-J., 1989. Geochemistry of recent TOC-rich sediments from the Gulf of California and the Black Sea. *Geol. Rundsch.,* 78:851–882. **doi:10.1007/BF01829327**

Brumsack, H.-J., 2006. The trace metal content of recent organic carbon-rich sediments: implications for Cretaceous black shale formation. *Palaeogeogr., Palaeoclimatol., Palaeoecol.,* 232:344-361. **doi:10.1016/j.palaeo.2005.05.011**

Brumsack, H.-J., and Gieskes, J.M., 1983. Interstitial water trace-metal chemistry of laminated sediments from the Gulf of California, Mexico. *Mar. Chem.,* 14:89–106. **doi:10.1016/0304-4203(83)90072-5**

Brumsack, H.-J., Heydemann, A., Kühn, V., Rachold, V., and Usdowski, E., 1995. Geochemistry and mineralogy of middle Aptian sediments from the Lower Saxony Basin, NW Germany. *In* Kemper, E., and Weiss, W. (Eds.), *Dark-Coloured Interbeds of the Late Middle Aptian of Northwest Germany: A Contribution to the Analysis of Carbonate and Colour Cycles*. N Geol. Palaeontol., Abh., 196(2):235–255.

Canfield, D.E., Raiswell, R., and Bottrell, S., 1992. The reactivity of sedimentary iron minerals toward sulfide. *Am. J. Sci.,* 292:659–683.

Church, T.M., and Wolgemuth, K., 1972. Marine barite saturation. *Earth Planet. Sci. Lett.,* 15:35–44. **doi:10.1016/0012-821X(72)90026-X**

Dellwig, O., Hinrichs, J., Hild, A., and Brumsack, H.-J., 2000. Changing sedimentation in tidal flat sediments of the southern North Sea from the Holocene to the present: a geochemical approach. *J. Sea Res.* 44(3–4):195–208. **doi:10.1016/S1385-1101(00)00051-4**

Dymond, J., Suess, E., and Lyle, M., 1992. Barium in deep-sea sediment: a geochemical proxy for paleoproductivity. *Paleoceanography,* 7:163–181.

Eagle, M., Paytan, A., Arrigo, K.R., van Dijken, G., and Murray, R.W., 2003. A comparison between excess barium and barite as indicators of carbon export. *Paleoceanography,* 18(1). **doi:10.1029/2002PA000793**

Erbacher, J., Mosher, D.C., Malone, M.J., et al., 2004. *Proc. ODP, Init. Repts.,* 207: College Station, TX (Ocean Drilling Program). **doi:10.2973/odp.proc.ir.207.2004**

Manheim, F.T., and Sayles, F.L., 1974. Composition and origin of interstitial waters of marine sediments, based on deep sea drill cores. *In* Goldberg, E.D. (Ed.), *The Sea* (Vol. 5): *Marine Chemistry: The Sedimentary Cycle:* New York (Wiley), 527–568.

McLennan, S.M., 1989. Rare earth elements in sedimentary rocks: influence of provenance and sedimentary processes. *In* Lipin, B.R., and McKay, G.A. (Eds.), *Geochemistry and Mineralogy of the Rare Earth Elements*. Rev. Mineral., 21:169–200.

McManus, J., Berelson, W.M., Klinkhammer, G.P., Johnson, K.S., Coale, K.H., Anderson, R.F., Kumar, N., Burdige, D.J., Hammond, D.E., Brumsack, H.-J., McCorkle, D.C., and Rushdi, A., 1998. Geochemistry of barium in marine sediments: implications for its use as a paleoproxy. *Geochim. Cosmochim. Acta,* 62:3453–3473. **doi:10.1016/S0016-7037(98)00248-8**

Paytan, A., Kastner, M., and Chavez, F., 1996. Glacial to interglacial fluctuations in productivity in the equatorial Pacific as indicated by marine barite. *Science,* 274:1355–1357. **doi:10.1126/science.274.5291.1355**

Potter, P.E., 1997. The Mesozoic and Cenozoic paleodrainage of South America: a natural history. *J. South Am. Earth Sci.,* 10(5–6):331–344. **doi:10.1016/S0895-9811(97)00031-X**

Prakash Babu, C., Brumsack, H.-J., and Schnetger, B., 1999. Distribution of organic carbon in surface sediments along the eastern Arabian Sea: a revisit. *Mar. Geol.,* 162:91–103. **doi:10.1016/S0025-3227(99)00047-X**

Quinby-Hunt, M.S., and Wilde, P., 1994. Thermodynamic zonation in the black shale facies based on iron-manganese-vanadium content. *Chem. Geol.,* 113(3–4):297–317. **doi:10.1016/0009-2541(94)90072-8**

Schmitz, B., 1987. Barium, equatorial high productivity, and the northward wandering of the Indian continent. *Paleoceanography,* 2:63–77.

Taylor, S.R., and McLennan, S.M., 1985. *The Continental Crust: Its Composition and Evolution:* Oxford (Blackwell Scientific).

Thurow, J., Brumsack, H.-J., Rullkötter, J., Littke, R., and Meyers, P., 1992. The Cenomanian/Turonian boundary event in the Indian Ocean—a key to understanding the global picture. *In* Duncan, R.A., Rea, D.K., Kidd, R.B., von Rad, U., and Weissel, J.K. (Eds.), *Synthesis of Results from Scientific Drilling in the Indian Ocean*. Geophys. Monogr., 70:253–273.

Tissot, B.P., and Welte, D.H., 1984. *Petroleum Formation and Occurrence* (2nd ed.): Heidelberg (Springer-Verlag).

Torres, M.E., Brumsack, H.-J., Bohrmann, G., and Emeis, K.C., 1996. Barite fronts in continental margin sediments: a new look at barium remobilization in the zone of sulfate reduction and formation of heavy barites in diagenetic fronts. *Chem. Geol.,* 127:125–139. **doi:10.1016/0009-2541(95)00090-9**

Wedepohl, K.H., 1971. Environmental influences on the chemical composition of shales and clays. *In* Ahrens, L.H., Press, F., Runcorn, S.K., and Urey, H.C. (Eds.), *Physics and Chemistry of the Earth:* Oxford (Pergamon), 8:305–333. **doi:10.1016/0079-1946(71)90020-6**

Wilde, P., Quinby-Hunt, M.S., and Erdtmann, B.-D., 1996. The whole-rock cerium anomaly: a potential indicator of eustatic sea-level changes in shales of the anoxic facies. *Sediment. Geol.,* 101(1–2):43–53. **doi:10.1016/0037-0738(95)00020-8**

APPENDIX

The precision and accuracy of analyzed elements are shown in Table AT1.

Major element concentrations in the sediments of Demerara Rise using pore water squeezing residues are shown in Table AT2.

Trace element concentrations in the sediments of Demerara Rise using pore water squeezing residues are shown in Table AT3.

REE concentrations in the sediments of Demerara Rise (Site 1258) using pore water squeezing residues are shown in Table AT4.

Figure F1. Map of Demerara Rise (Online Map Creation www.aquarius.geomar.de).
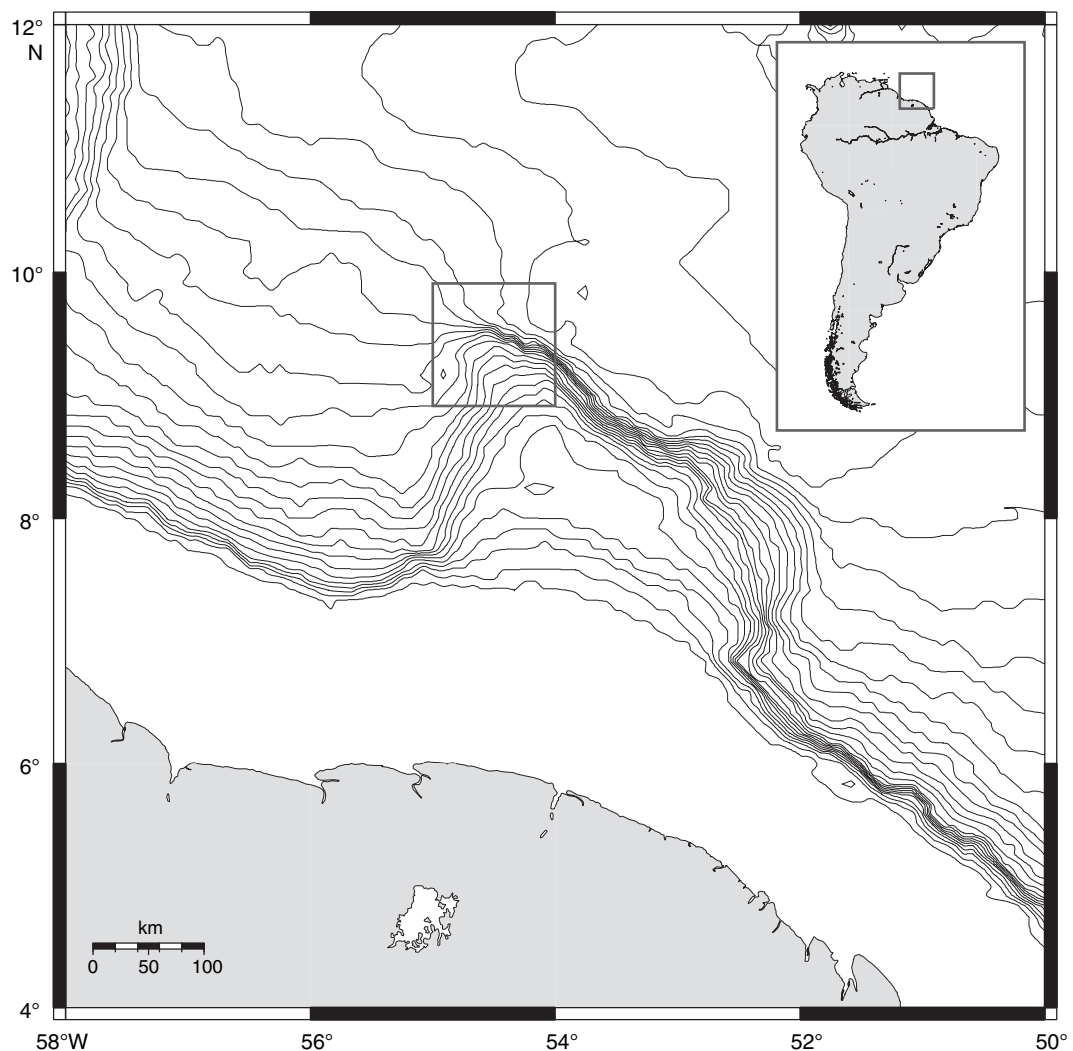
Figure F2. Major components of sediments from Demerara Rise in the system $Al_2O_3 \times 5$-SiO_2-$CaO \times 2$ (relative weight ratios). Data point for average shale (AS) (Wedepohl, 1971) also shown for comparison. **A.** Unit I. **B.** Unit II–IV. **C.** Unit V.
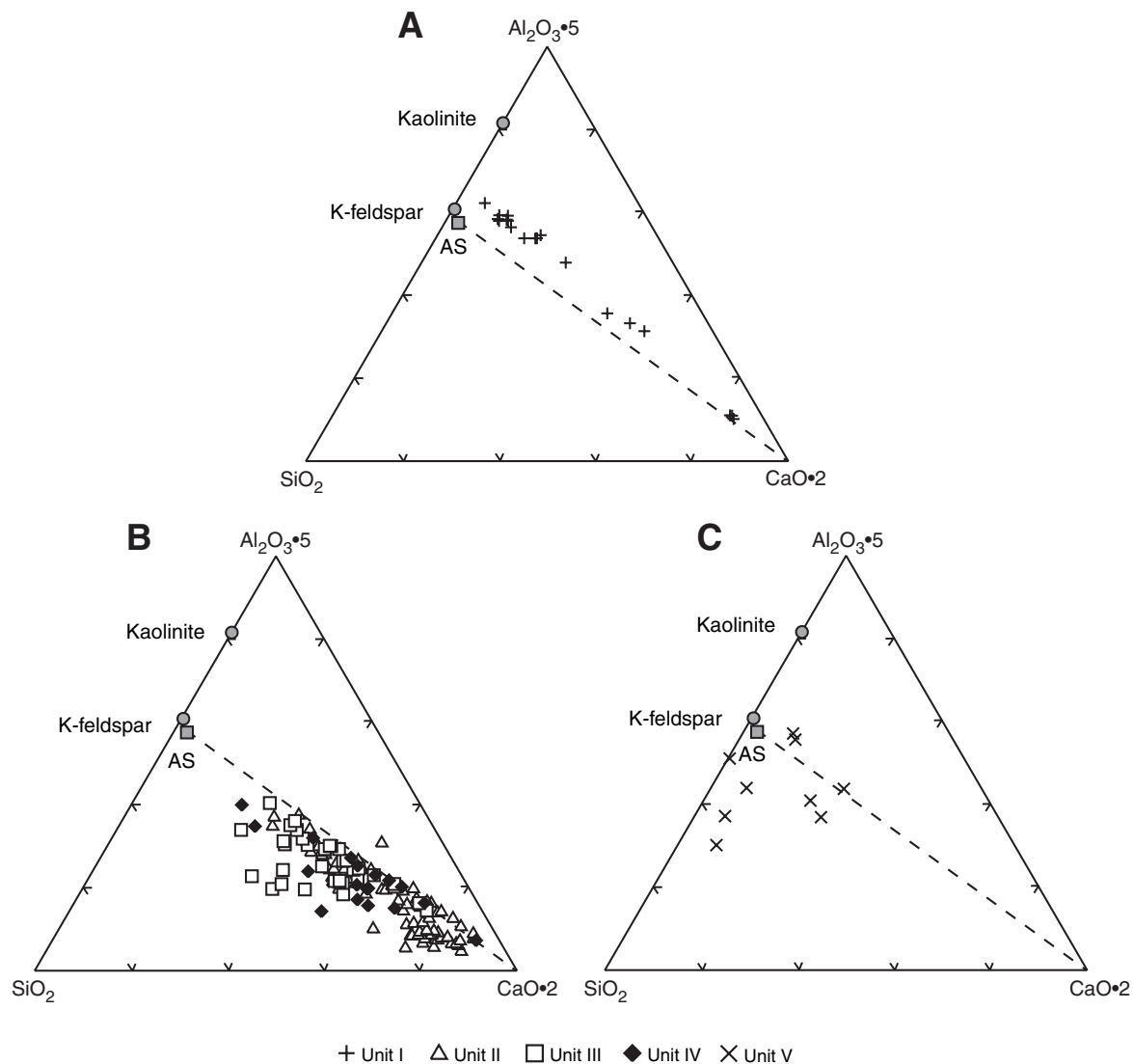
Figure F3. Proportion of major components of lithologic Units I–V. OM = organic matter. For calculations, see Table T1, p. 26.
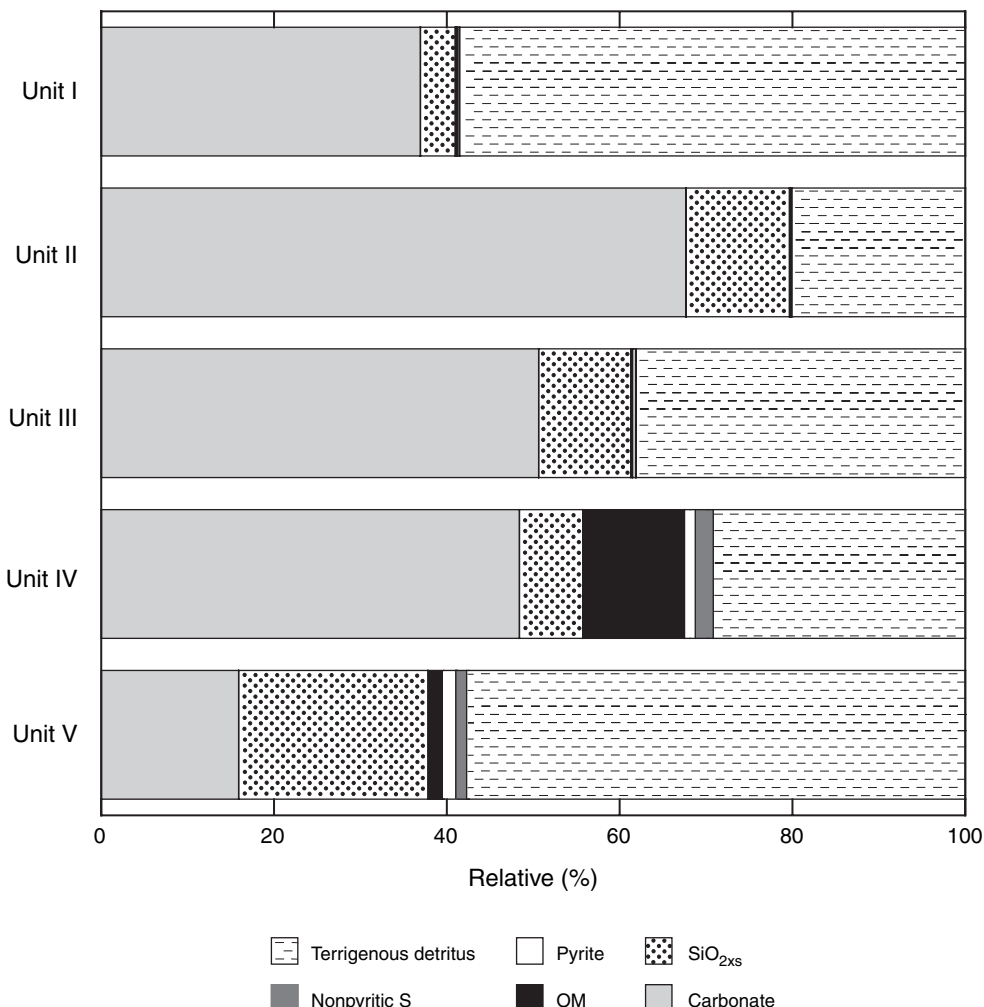
Figure F4. Correlation of two calculation methods for terrigenous detritus: (1) see Table T1, p. 26, (2) sum of measured concentrations.
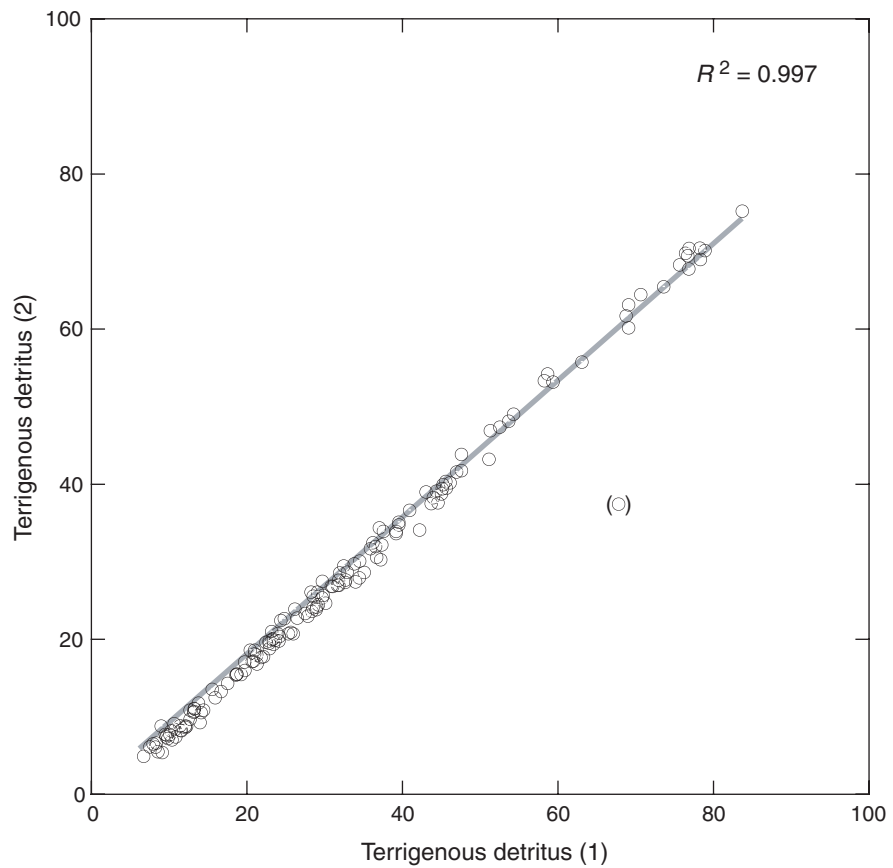
Figure F5. Comparison of values of weathering factor (WF) and chemical index of alteration (CIA) for Units I–V. AS = average shale.
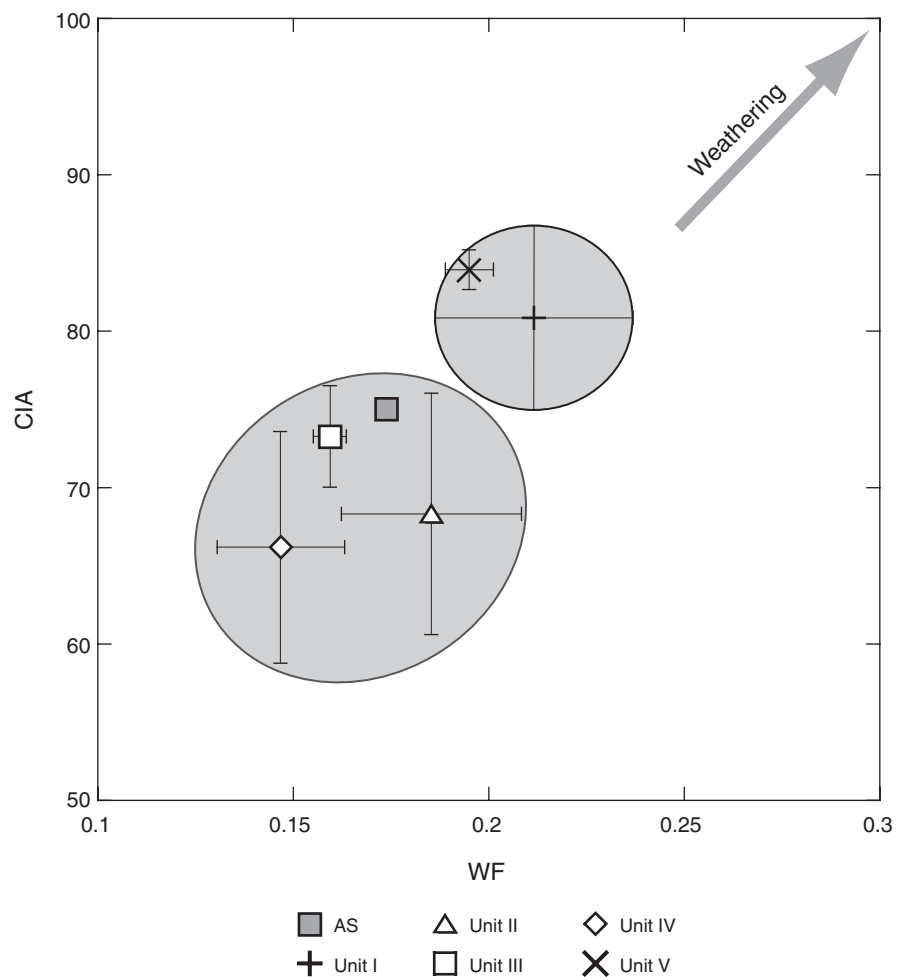
Figure F6. Scatter plots for heavy minerals indicating elements vs. major components. Samples are calculated carbonate-free. AS = average shale. **A.** TiO_2 vs. Al_2O_3. **B.** Zr vs. Al_2O_3. **C.** TiO_2 vs. SiO_{2xs}. **D.** Zr vs. SiO_{2xs}.
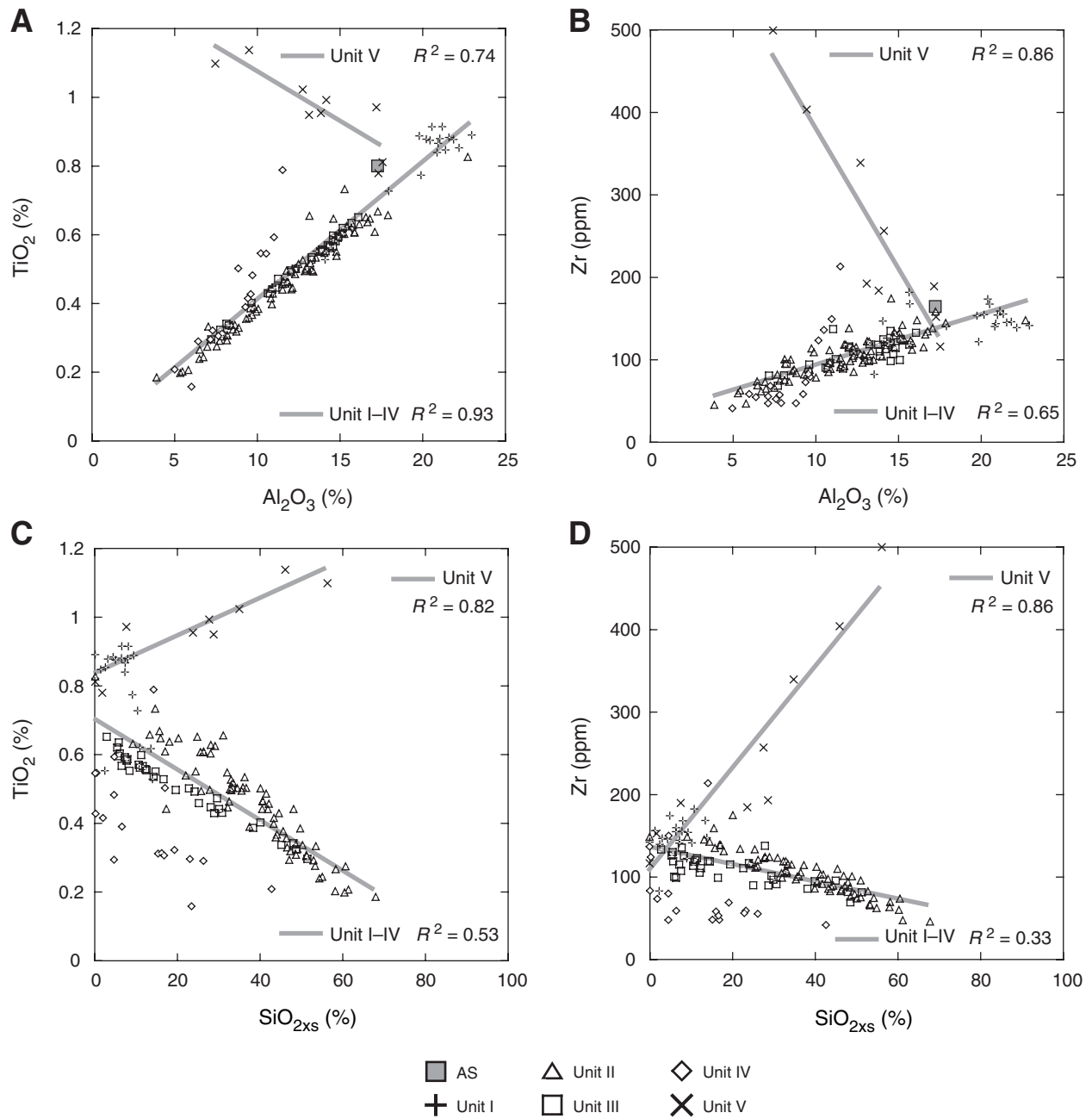
Figure F7. Average rare earth element (REE) distribution patterns for Units I–V. Element/Al ratios are normalized to element/Al ratios of Upper Continental Crust (UCC) (Taylor and McLennan, 1985). Post-Archean average Australian Shale (PAAS) (Taylor and McLennan, 1985) also shown for comparison.
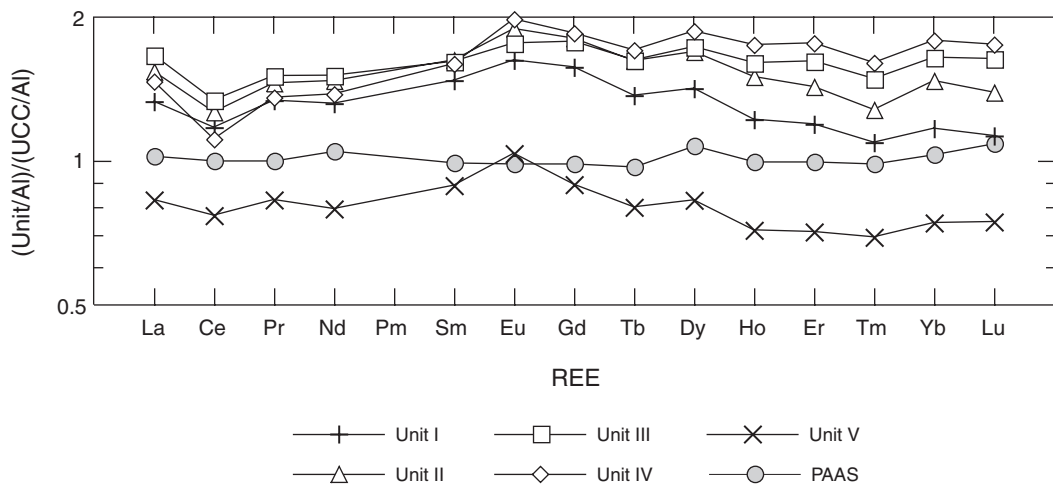
Figure F8. Scatter plots of carbonate chemistry. **A.** CaO vs. total inorganic carbon (TIC). **B.** Sr vs. TIC. **C.** MgO vs. TIC. **D.** MnO vs. TIC.
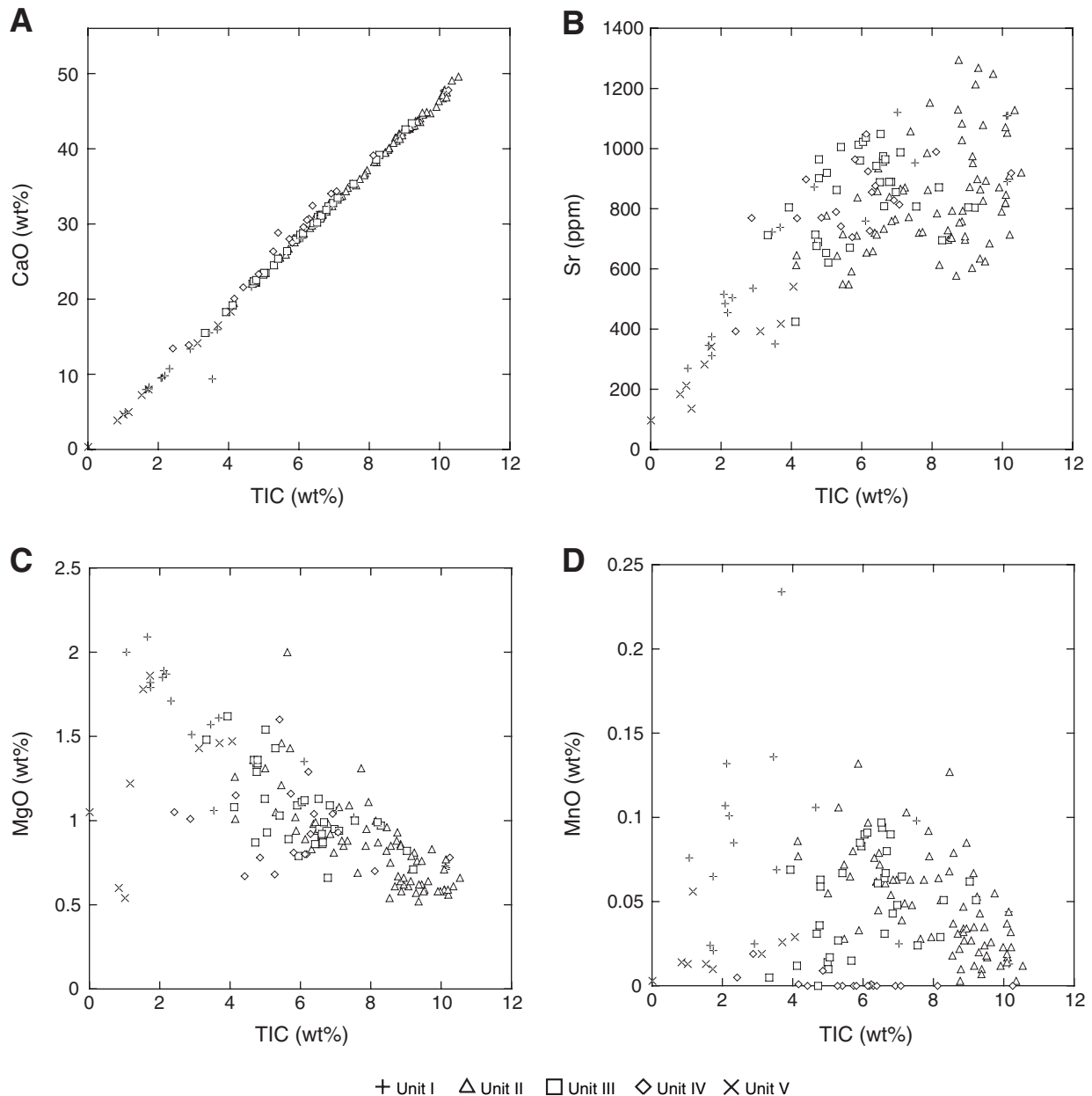
Figure F9. Mean values of element/Al ratios of Ca, Sr, Mg and Mn in Units I–V. Element/Al ratios in AS are indicated by dashed line.
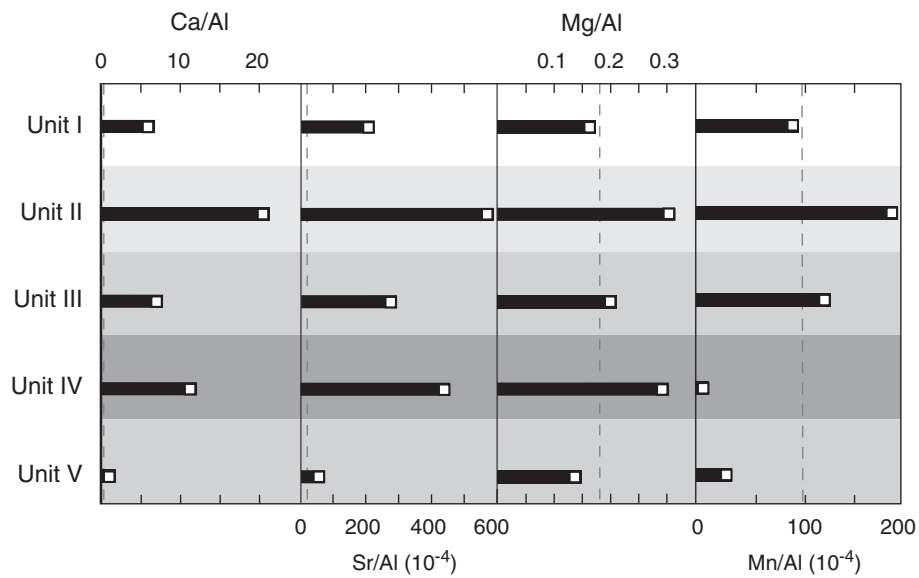
Figure F10. Degree of pyritization of sediments from Demerara Rise in the Fe_x-total organic carbon (TOC)-S × 2 (following stoichiometry of pyrite-FeS_2) system (relative weight ratios). Reactive Fe (Fe_x) is calculated with $Fe_x = Fe - 0.25 \times Al$. Data point for pyrite is also shown.
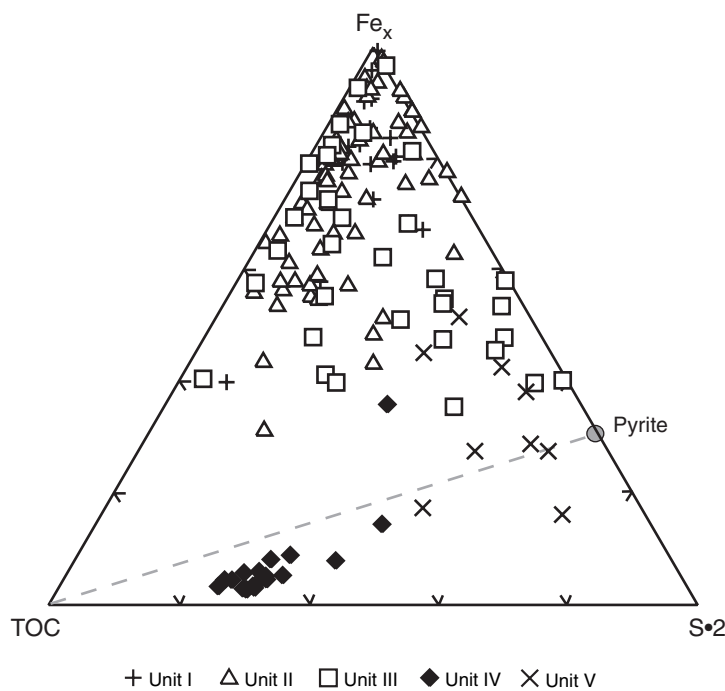
Figure F11. Mean values of TM/Al ratios of diagnostic TM in Units I–V. TM are presented in order of TM enrichment relative to AS (dashed line) in Unit IV.
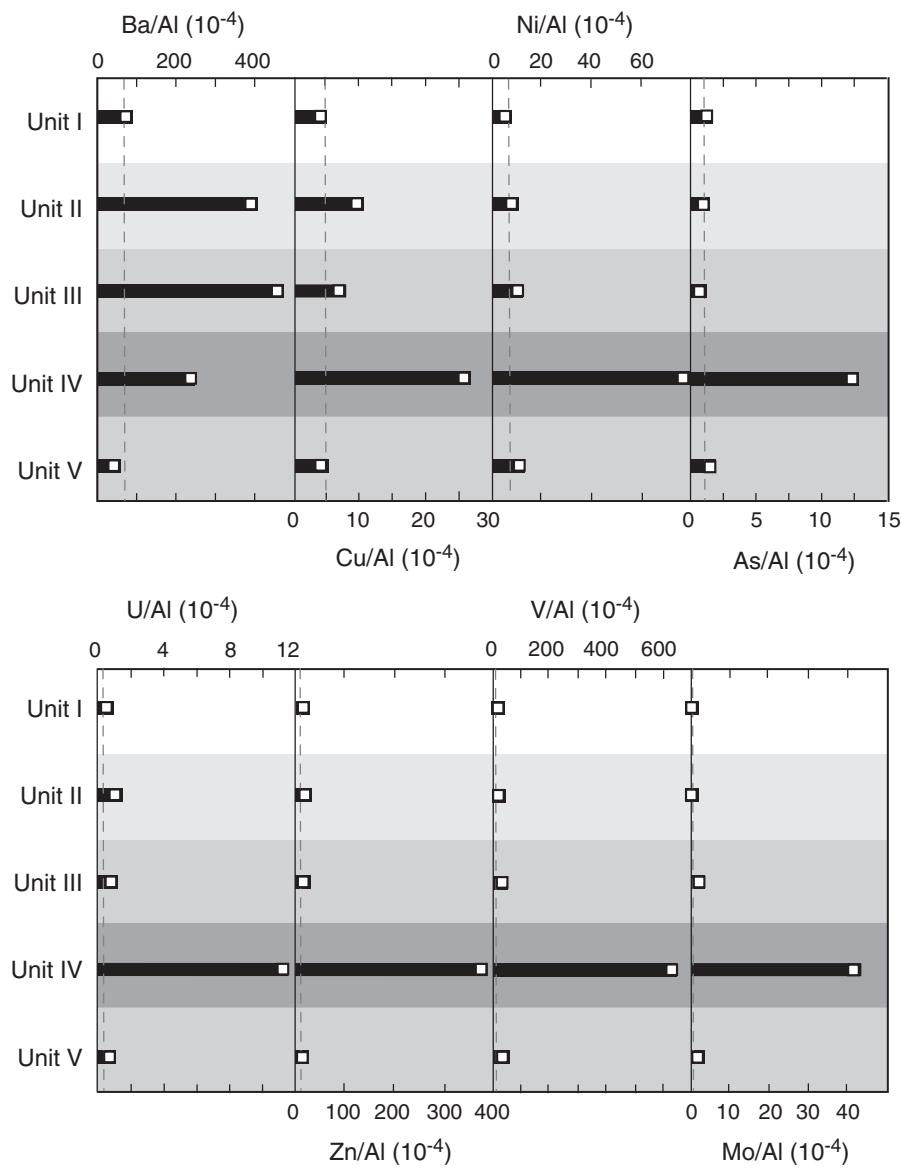
Table T1. Calculation of proportions of major components
presented in Figure F3, p. 17.

Carbonate	[%] = TIC [wt%] $\times$ 8.3331
SiO_{2xs}	[%] = SiO_2 [wt%] – Al_2O_3 [wt%] $\times$ $(SiO_2/Al_2O_3)_{min/Unit}$
OM	[%] = TOC [wt%] $\times$ 1.34
Pyrite	[%] = min $(pyrite_{Fe}$ [wt%]; $pyrite_{TS}$ [wt%])
If $pyrite_{Fe}$ [%] < $pyrite_{TS}$ [%]	
nonpyrite S	[%] = TS [wt%] – S_{pyrite} [wt%]
terrigenous detritus	[%] = 100% – Σ(carbonate; SiO_{2xs}; OM; pyrite; nonpyritic S)

Notes: OM = organic matter. TIC = total inorganic carbon. TOC = total
organic carbon. TS = total sulfur.

Table T2. Ce anomaly for lithologic Units I–V.

		Unit I	Unit II	Unit III	Unit IV	Unit V
Taylor and McLennan (1985)	Ce* = $\sqrt{(La \times Pr)}$	1.33	1.49	1.58	1.41	0.83
	Ce/Ce*	0.88	0.85	0.85	0.79	0.93
Wilde et al. (1996)	Ce* = (La + Pr)/2	1.33	1.49	1.58	1.41	0.83
	log Ce/Ce*	–0.06	–0.07	–0.07	–0.1	–0.03

Note: Two quantification approaches are given.

Table AT1. Precision and accuracy of analyzed elements.

Element	Method	Precision SD (1σ) (rel%)	Accuracy (rel%)
TS	IR analyzer	2.7	102.6
TC	IR analyzer	1.3	100.5
TIC	Coulometry	0.8	99.8
SiO_2	XRF	0.4	99.7
TiO_2	XRF	1.0	102.8
Al_2O_3	XRF	0.5	99.9
Fe_2O_3	XRF	0.4	100.6
MnO	XRF	1.4	101.5
MgO	XRF	0.6	108.7
CaO	XRF	0.5	100.4
Na_2O	XRF	0.0	98.9
K_2O	XRF	1.4	92.7
P_2O_5	XRF	0.7	103.4
As	XRF	2.7	93.8
Ba	XRF	3.0	104.7
Co	XRF	5.4	98.1
Cr	XRF	3.6	108.8
Cu	XRF	3.7	89.8
Mo	XRF	4.7	101.6
Ni	XRF	0.8	99.0
Pb	XRF	9.0	93.6
Rb	XRF	2.0	98.2
Sr	XRF	0.5	102.5
U	XRF	8.8	105.5
V	XRF	1.2	104.3
Y	XRF	3.0	100.7
Zn	XRF	1.7	97.8
Zr	XRF	2.8	103.0
REE	ICP-MS	6.8*	95.9–102.6[†]

Notes: Accuracy is defined as 100% times the mean of the repeat analyses divided by the expected value. Precision is defined as 100% times the best estimate standard deviation (1σ) divided by the mean of the repeats. SD = standard deviation. REE = rare earth element. IR = infrared, XRF = X-ray fluorescence, ICP-MS = inductively coupled–plasma mass spectrometry. * = maximum value. † = range.

Table AT2. Major element concentrations in sediments of Demerara Rise using pore water squeezing residues. (**See table notes.** Continued on next three pages.)

Hole, core, section, interval (cm)	Unit	Depth		Bulk parameter (wt%)			Major element oxide (wt%)									
		(mbsf)	(mcd)	TS	TIC	TOC	SiO$_2$	TiO$_2$	Al$_2$O$_3$	Fe$_2$O$_3$	MnO	MgO	CaO	Na$_2$O	K$_2$O	P$_2$O$_5$
207-																
1257A-1H-1, 145–150	I	1.45	1.45	0.03	1.65	0.06	46.47	0.669	17.11	6.36	0.024	2.09	7.97	1.29	2.41	0.069
1257A-2H-4, 145–150	II	8.55	8.55	0.06	7.94	0.08	18.63	0.187	4.98	2.06	0.029	1.11	37.13	0.93	0.81	0.099
1257A-3H-4, 145–150	II	18.05	18.05	0.03	8.85	0.18	14.52	0.131	3.47	1.34	0.034	0.86	41.98	0.94	0.65	0.086
1257A-4H-3, 145–150	II	26.05	26.05	0.08	8.85	0.00	14.04	0.130	3.50	1.44	0.032	0.85	41.97	0.83	0.64	0.137
1257A-5H-3, 145–150	II	35.55	35.55	0.02	7.39	0.18	21.85	0.234	5.78	2.31	0.048	1.09	34.79	0.87	0.68	0.100
1257A-6X-3, 145–150	II	45.05	45.05	0.04	9.07	0.04	16.82	0.060	1.63	0.66	0.027	0.61	42.53	0.60	0.15	0.060
1257A-7X-3, 145–150	II	49.35	49.35	0.03	9.45	0.01	14.63	0.059	1.59	0.62	0.024	0.62	44.05	0.66	0.21	0.065
1257B-3R-2, 145–150	II	52.75	56.12	0.01	9.15	0.22	15.62	0.095	2.57	0.92	0.035	0.71	42.66	0.56	0.25	0.057
1257B-8X–3, 145–150	II	58.55	58.55	0.05	7.63	0.02	26.69	0.076	2.10	1.04	0.028	0.69	35.12	0.69	0.18	0.061
1257B-4R-3, 143–150	II	63.82	70.93	0.02	8.46	0.24	16.89	0.132	3.56	1.64	0.127	0.96	39.55	0.94	0.84	0.108
1257B-5R-4, 42–49	II	73.65	76.70	0.02	7.88	0.16	20.47	0.172	4.44	1.73	0.077	0.95	36.74	1.01	0.88	0.102
1257B-7R-2, 143–150	III	91.23	95.60	0.04	6.61	0.19	29.92	0.194	4.81	1.63	0.064	0.91	31.21	1.03	0.77	0.080
1257B-8R-4, 142–150	III	103.79	107.22	0.05	5.95	0.21	33.34	0.232	5.86	1.51	0.083	0.79	28.09	1.31	1.24	0.082
1257B-9R-3, 140–150	III	112.02	113.79	0.02	6.54	0.21	27.90	0.253	6.30	2.15	0.094	0.95	30.92	1.28	1.21	0.085
1257A-14X-4, 140–150	III	117.70	117.70	0.02	5.91	0.17	30.98	0.284	7.03	2.62	0.085	1.09	27.92	1.32	1.28	0.080
1257A-10R-4, 140–150	III	123.10	125.68	0.01	6.04	0.25	29.52	0.290	7.29	2.74	0.090	1.11	28.56	1.28	1.20	0.077
1257A-15X-5, 140–150	III	128.90	128.49	0.02	6.12	0.18	29.14	0.291	7.26	2.58	0.091	1.12	28.76	1.33	1.18	0.078
1257B-11R-4, 140–150	III	132.70	135.28	0.02	3.93	0.12	39.76	0.407	10.13	4.40	0.069	1.62	18.27	1.67	1.45	0.082
1257B-12R-3, 140–150	III	140.60	143.27	1.52	4.79	0.04	34.66	0.342	8.73	4.55	0.063	1.34	22.19	1.58	1.38	0.087
1257B-13R-4, 140–150	III	151.70	154.90	0.38	6.84	0.14	26.16	0.231	5.69	2.14	0.043	1.09	32.34	1.22	0.99	0.063
1257C-8R-6, 90–100	III	157.50	159.95	0.06	6.61	0.20	30.65	0.199	4.87	1.23	0.031	0.92	30.71	1.26	0.88	0.054
1257A-18X-4, 140–150	III	156.16	161.96	0.18	5.29	0.13	35.32	0.309	7.69	2.40	0.027	1.43	24.50	1.40	1.29	0.078
1257C-9R-6, 51–61	III	166.15	168.56	0.18	5.67	0.03	39.10	0.179	4.34	1.45	*0.015*	0.89	26.40	1.24	0.77	0.105
1257C-10R-1, 140–150	III	169.80	172.21	0.31	3.33	0.08	48.33	0.324	7.97	2.41	*0.005*	1.48	15.51	1.64	1.44	0.189
1257C-12R-2, 90–100	IV	190.10	192.65	2.01	5.41	3.51	24.26	0.088	3.27	6.52	*0.000*	1.60	28.82	0.90	1.53	2.713
1257C-13R-2, 140–150	IV	200.20	202.75	1.34	5.27	6.03	33.66	0.118	2.77	0.90	*0.000*	0.68	26.34	1.32	0.52	0.990
1257C-15R-3, 17–27	IV	218.98	221.53	1.44	6.29	7.71	23.09	0.139	3.03	1.20	*0.000*	0.92	30.68	1.06	0.49	0.945
1257B-27R-3, 0–7	V	225.30	228.94	1.50	3.12	0.41	47.12	0.708	10.20	4.88	*0.019*	1.43	14.15	0.88	1.12	0.150
1257C-16R-6, 20–30	V	233.87	235.03	1.08	3.70	0.40	46.08	0.658	9.04	4.37	0.026	1.46	16.53	0.84	1.04	0.147
1257A-31X–1, 71–81	V	275.81	281.61	0.93	4.06	1.04	37.93	0.644	11.34	5.49	0.029	1.47	18.35	0.85	1.32	0.120
1258A-1R-1, 145–150	I	1.45	1.45	0.02	6.11	0.00	24.90	0.358	8.78	5.89	0.090	1.35	28.11	0.87	0.85	0.154
1258A-1R-2, 145–150	I	2.95	2.95	0.03	7.52	0.17	18.50	0.317	7.96	2.80	0.098	1.02	35.40	0.71	0.64	0.097
1258A-3R-4, 145–150	II	20.15	20.15	0.05	8.94	0.13	17.69	0.052	1.38	0.67	0.085	0.62	42.24	0.58	0.17	0.086
1258A-4R-4, 145–150	II	29.75	29.75	0.04	8.85	0.03	17.84	0.088	1.83	0.77	0.047	0.64	41.68	0.67	0.28	0.081
1258A-5R-3, 145–150	II	37.65	42.15	0.03	7.73	0.13	21.13	0.184	4.42	1.59	0.063	1.31	35.99	1.13	1.27	0.099
1258A-6R-4, 145–150	II	48.75	49.27	0.00	5.63	0.00	30.97	0.349	6.95	3.39	0.065	2.00	25.93	1.32	1.68	0.095
1258A-7R-4, 145–150	II	58.15	59.14	0.03	5.71	0.06	31.11	0.277	6.65	3.05	0.080	1.43	26.70	1.35	1.63	0.115
1258A-8R-4, 140–150	II	68.07	69.92	0.04	6.14	0.02	31.54	0.228	5.62	1.85	0.097	0.89	28.71	1.56	1.58	0.095
1258A-9R-6, 140–150	II	80.80	81.05	0.05	5.46	0.00	33.87	0.275	6.68	2.31	0.072	1.21	25.55	1.48	1.70	0.112
1258A-10R-3, 140–150	II	86.00	86.63	0.02	5.30	0.06	33.86	0.290	7.34	2.77	0.106	1.05	24.56	1.47	1.66	0.091
1258A-11R-5, 135–145	II	98.65	98.35	0.01	4.14	0.00	40.07	0.360	9.17	3.35	0.086	1.26	19.55	1.84	1.85	0.092
1258A-12R-5, 140–150	II	108.30	108.69	0.02	4.15	0.02	40.69	0.325	8.38	2.56	0.077	1.01	19.47	1.91	1.94	0.106
1258A-13R-4, 140–150	II	116.40	117.01	0.02	5.86	0.16	32.14	0.259	6.63	2.49	0.132	1.02	27.62	1.32	1.11	0.101
1258B-14R-4, 140–150	II	133.80	134.22	0.05	6.32	0.14	31.80	0.204	5.15	1.64	0.076	0.83	29.47	1.10	0.83	0.082
1258B-18R-3, 140–150	II	170.90	171.49	0.04	6.63	0.22	31.54	0.173	4.47	1.48	0.061	0.86	30.94	0.83	0.42	0.069
1258A-17R-4, 140–150	II	154.95	176.79	0.03	6.37	0.20	30.78	0.236	5.76	2.05	0.062	0.98	29.77	0.99	0.67	0.073

Table AT2 (continued).

A. Hetzel et al.
Inorganic Geochemical Characterization of Lithologic Units

30

Hole, core, section, interval (cm)	Unit	Depth (mbsf)	(mcd)	Bulk parameter (wt%) TS	TIC	TOC	Major element oxide (wt%) SiO₂	TiO₂	Al₂O₃	Fe₂O₃	MnO	MgO	CaO	Na₂O	K₂O	P₂O₅
1258A-20R-2, 140–150	II	181.00	204.43	0.04	6.45	0.21	32.53	0.205	4.95	1.65	0.079	0.86	30.17	0.96	0.59	0.091
1258A-22R-3, 140–150	II	201.50	224.93	0.02	6.47	0.14	29.64	0.247	6.21	2.22	0.072	0.94	30.19	0.92	0.64	0.073
1258A-24R-3, 139–150	II	220.69	244.12	0.13	7.23	0.23	24.27	0.249	6.10	1.88	0.103	0.85	33.71	0.80	0.68	0.078
1258A-26R-2, 140–150	II	238.50	260.95	0.02	5.00	0.14	34.53	0.381	9.63	3.41	0.055	1.31	23.44	1.23	1.00	0.103
1258A-28R-5, 145–150	II	262.35	284.80	0.01	8.57	0.11	16.91	0.174	4.52	1.58	0.079	0.85	40.13	0.72	0.50	0.057
1258A-30R-2, 140–150	II	277.10	299.47	0.02	7.10	0.20	24.22	0.249	6.46	2.31	0.039	1.08	33.23	1.03	0.77	0.068
1258A-32R-5, 140–150	II	300.90	324.11	0.03	8.21	0.19	18.84	0.191	4.80	1.96	0.051	0.87	38.20	0.82	0.66	0.051
1258A-33R-4, 140–150	II	307.00	329.81	0.01	5.47	0.05	33.10	0.343	8.56	3.18	0.028	1.46	25.52	1.19	1.09	0.079
1258B-36R-3, 90–100	III	334.00	346.81	0.03	4.99	0.18	43.12	0.236	5.60	1.94	*0.014*	1.13	23.28	0.99	0.82	0.089
1258A-35R-3, 140–150	III	326.80	349.67	0.21	6.97	0.15	25.90	0.209	5.02	1.93	0.048	0.95	32.80	0.86	0.65	0.060
1258A-37R-2, 145–150	III	344.65	367.52	0.06	5.05	0.22	44.26	0.199	4.67	1.46	*0.017*	0.93	23.47	0.94	0.65	0.067
1258A-39R-1, 63–73	III	361.53	382.27	0.27	4.76	0.01	40.07	0.298	7.24	2.45	0.036	1.29	22.28	1.15	1.00	0.113
1258B-39R-5, 135–150	III	366.35	384.10	0.25	4.68	0.18	40.25	0.307	7.48	2.52	0.031	1.36	22.04	1.11	1.07	0.103
1258B-43R-2, 110–120	III	390.40	412.51	0.52	4.12	0.10	49.73	0.214	5.05	2.00	*0.012*	1.08	19.18	0.98	0.73	0.140
1258B-45R-2, 75–85	IV	399.25	420.08	3.41	4.17	15.14	25.34	0.256	6.02	2.10	*0.001*	1.15	20.08	1.56	1.10	0.188
1258B-46R-1, 31–44	IV	403.41	425.47	4.67	2.87	12.03	36.30	0.384	6.69	3.72	*0.019*	1.01	13.89	1.67	1.00	0.119
1258B-51R-2, 20–29	IV	427.92	452.24	1.86	6.23	9.17	18.46	0.233	4.64	1.91	*0.001*	1.29	30.52	0.86	0.80	0.909
1258B-52R-2, 70–80	IV	433.71	458.03	1.70	6.92	9.68	14.22	0.182	4.04	1.55	*0.000*	1.04	34.02	0.77	0.62	0.982
1258B-54R-3, 0–10	IV	444.38	468.86	1.95	5.73	8.57	22.48	0.311	5.72	2.12	*0.000*	1.16	28.01	0.70	0.79	0.951
1258B-55R-3, 58–68	IV	448.27	475.13	3.03	2.42	5.69	43.41	0.631	9.16	4.46	*0.005*	1.05	13.45	0.65	1.17	1.741
1258C-30R-1, 112–122	V	462.52	495.02	3.29	1.53	4.53	44.37	0.710	15.28	6.12	*0.013*	1.78	7.24	1.00	1.45	0.083
1258C-34R-2, 135–150	V	483.55	516.05	3.34	1.73	2.65	44.41	0.669	14.78	7.75	*0.010*	1.86	7.99	1.07	1.44	0.073
1259A-1R-2, 105–110	I	2.55	2.55	0.04	10.12	0.18	7.15	0.083	2.20	0.92	*0.015*	0.73	47.72	0.66	0.28	0.220
1259A-2R-2, 145–150	I	11.75	11.75	0.03	10.14	0.06	7.59	0.096	2.43	0.91	0.044	0.71	47.62	0.61	0.28	0.153
1259A-3R-4, 145–150	I	24.25	24.25	0.02	10.15	0.35	7.12	0.096	2.41	0.83	*0.013*	0.72	47.87	0.61	0.28	0.122
1259A-5R-2, 145–150	II	39.35	39.35	0.02	10.54	0.26	5.20	0.077	1.96	0.97	*0.012*	0.66	49.58	0.63	0.24	0.071
1259A-6R-2, 145–150	II	48.45	48.45	0.04	10.14	0.36	7.18	0.114	2.36	1.16	0.044	0.77	47.75	0.69	0.28	0.070
1259A-7R-4, 145–150	II	60.55	60.55	0.03	10.09	0.01	8.03	0.105	2.84	0.99	0.037	0.71	46.70	0.68	0.33	0.084
1259A-8R-4, 145–150	II	69.75	69.75	0.01	9.74	0.10	9.89	0.115	3.21	1.43	0.055	0.83	44.72	0.68	0.31	0.084
1259A-9R-5, 145–150	II	80.35	80.35	0.03	9.24	0.06	12.11	0.147	3.82	1.42	0.053	0.81	43.01	0.73	0.36	0.089
1259A-10R-5, 140–150	II	90.00	90.00	0.01	9.32	0.17	11.34	0.145	3.74	1.31	0.043	0.76	43.69	0.76	0.45	0.073
1259A-12R-5, 140–150	II	109.40	109.40	0.06	10.35	0.35	5.81	0.061	1.65	0.61	*0.003*	0.61	49.07	0.80	0.33	0.118
1259A-14R-3, 140–150	II	125.70	125.70	0.02	9.45	0.22	10.73	0.138	3.09	1.47	0.035	0.76	43.55	0.66	0.35	0.219
1259A-16R-1, 140–150	II	142.00	142.00	0.02	10.10	0.20	9.13	0.062	1.54	0.57	*0.017*	0.59	47.46	0.66	0.33	0.078
1259A-18R-1, 135–145	II	161.15	161.15	0.03	9.37	0.16	13.90	0.079	2.07	0.81	*0.010*	0.62	43.77	0.58	0.16	0.078
1259A-20R-4, 130–140	II	185.00	185.00	0.03	10.09	0.11	10.17	0.047	1.29	0.51	*0.014*	0.58	47.10	0.61	0.23	0.065
1259A-22R-3, 140–150	II	202.90	202.90	0.00	9.53	0.12	13.19	0.076	1.98	0.73	*0.017*	0.59	44.55	0.75	0.28	0.086
1259A-24R-1, 132–142	II	219.12	219.12	0.02	9.37	0.11	15.67	0.044	1.16	0.49	*0.007*	0.52	43.60	0.57	0.17	0.099
1259A-26R-5, 140–150	II	244.30	244.30	0.01	10.21	0.09	10.10	0.036	0.96	0.38	0.023	0.56	47.49	0.67	0.15	0.054
1259A-29R-4, 140–150	II	271.70	271.70	0.02	8.94	0.15	17.18	0.078	1.99	0.78	0.034	0.66	41.78	0.71	0.16	0.069
1259A-32R-1, 133–143	II	296.03	296.03	0.01	8.15	0.19	18.44	0.160	3.76	1.75	0.064	1.00	38.27	1.01	0.72	0.150
1259A-34R-2, 140–150	II	316.92	316.77	0.02	5.88	0.05	30.68	0.258	6.57	2.57	0.033	0.94	27.56	1.61	1.28	0.126
1259A-36R-1, 140–150	II	334.70	335.30	0.01	7.34	0.17	25.52	0.162	4.18	1.83	0.063	0.88	34.34	0.98	0.50	0.096
1259A-38R-1, 140–150	II	354.00	354.83	0.03	6.79	0.10	28.20	0.202	5.09	2.06	0.054	0.98	31.63	1.09	0.58	0.090
1259A-40R-3, 90–100	III	375.70	374.85	0.05	6.42	0.19	31.65	0.201	4.92	1.85	0.061	0.86	30.08	0.96	0.47	0.074
1259A-43R-1, 140–150	III	402.10	403.27	0.03	5.41	0.09	34.67	0.291	7.25	2.50	0.067	1.03	25.37	1.43	0.98	0.078
1259A-45R-2, 140–150	III	422.90	424.38	0.01	6.68	0.12	26.91	0.254	6.30	2.38	0.080	0.99	31.23	1.28	0.85	0.121
1259A-48R-3, 138–150	III	453.18	453.19	0.01	9.21	0.25	13.48	0.129	3.27	1.14	0.051	0.71	43.40	0.74	0.48	0.044
1259A-50R-5, 137–149	III	475.06	475.59	0.07	7.55	0.12	21.88	0.218	5.38	1.62	0.024	1.00	35.32	1.00	0.85	0.091

A. Hetzel et al.
Inorganic Geochemical Characterization of Lithologic Units

31

Hole, core, section, interval (cm)	Unit	Depth		Bulk parameter (wt%)			Major element oxide (wt%)									
		(mbsf)	(mcd)	TS	TIC	TOC	SiO$_2$	TiO$_2$	Al$_2$O$_3$	Fe$_2$O$_3$	MnO	MgO	CaO	Na$_2$O	K$_2$O	P$_2$O$_5$
1259A-52R-1, 103–117	III	488.33	490.08	0.07	4.72	0.22	46.46	0.181	4.34	1.17	0.000	0.87	22.37	1.26	0.71	0.093
1259C-16R-5, 137–150	IV	525.65	529.18	1.29	7.07	7.63	18.30	0.133	2.97	0.99	0.000	0.93	34.36	1.08	0.56	0.384
1259C-17R-1, 136–146	IV	529.26	532.38	2.10	6.18	10.12	20.81	0.152	3.83	1.24	0.000	0.80	29.42	1.40	0.57	0.063
1259C-18R-4, 140–150	IV	543.40	547.73	4.52	4.86	18.55	17.55	0.176	4.23	2.49	0.009	0.78	23.33	1.23	0.72	0.185
1259C-19R-2, 78–88	V	549.22	551.57	1.50	0.01	0.54	68.50	0.994	14.10	3.61	0.003	1.05	0.34	0.75	1.97	0.080
1259B-25R-1, 89–100	V	554.09	555.18	0.44	1.16	0.26	64.80	0.926	11.46	3.87	0.056	1.22	4.99	0.67	1.47	0.072
1260A-1R-1, 58–63	I	0.58	0.58	0.07	1.74	0.34	46.13	0.761	16.87	6.23	0.021	1.79	8.29	1.37	2.37	0.086
1260A-2R-1, 145–150	II	2.45	2.45	0.02	7.86	0.00	16.33	0.286	7.82	3.23	0.092	0.85	36.48	0.62	0.67	0.085
1260A- 3R-1, 145–150	II	11.75	11.75	0.00	8.74	0.08	14.00	0.182	4.68	1.87	0.022	0.88	41.47	0.61	0.45	0.206
1260A-4R-3, 145–150	II	23.95	23.95	0.01	8.76	0.31	14.23	0.146	3.98	1.58	0.003	0.93	41.45	0.81	0.60	0.073
1260A-6R-5, 90–100	II	45.10	45.10	0.01	8.78	0.00	17.62	0.096	2.49	0.79	0.010	0.67	41.04	0.84	0.55	0.085
1260A-7R-5, 145–150	II	54.95	55.05	0.03	10.09	0.00	10.40	0.051	1.38	0.49	0.019	0.59	47.14	0.70	0.36	0.067
1260A-8R-5, 145–150	II	64.62	64.72	0.02	10.20	0.10	10.00	0.049	1.27	0.49	0.032	0.59	46.83	0.71	0.22	0.063
1260A-9R-5, 142–150	II	74.32	73.32	0.01	9.29	0.04	14.79	0.070	1.83	0.63	0.020	0.57	43.09	0.73	0.36	0.071
1260A-10R-5, 142–150	II	84.02	83.12	0.06	9.98	0.12	11.46	0.052	1.37	0.51	0.023	0.58	46.33	0.76	0.32	0.062
1260A-12R-4, 140–150	II	101.80	100.42	0.05	8.54	0.02	21.89	0.054	1.11	0.49	0.018	0.54	39.87	0.71	0.10	0.068
1260A-14R-6, 105–110	II	123.85	122.17	0.02	8.69	0.00	19.77	0.074	1.78	0.67	0.031	0.61	40.78	0.72	0.33	0.072
1260A-17R-1, 145–150	II	145.65	143.84	0.01	9.64	0.06	13.09	0.067	1.69	0.61	0.026	0.64	44.87	0.72	0.33	0.061
1260A-19R-5, 143–150	II	170.63	168.82	0.03	8.56	0.07	19.39	0.097	2.40	0.94	0.037	0.75	40.05	0.79	0.31	0.069
1260A-21R-1, 130–140	II	183.80	181.99	0.01	9.14	0.04	15.46	0.079	2.10	0.72	0.067	0.64	42.77	0.98	0.43	0.088
1260A-23R-2, 140–150	II	204.30	202.49	0.01	8.45	0.10	18.63	0.131	3.20	1.42	0.068	0.82	39.45	1.08	0.68	0.114
1260A-25R-2, 141–150	II	223.61	221.80	0.03	6.43	0.22	27.81	0.234	5.68	2.34	0.045	0.99	30.68	1.40	1.21	0.127
1260A-27R-4, 140–150	II	245.90	244.39	0.03	6.95	0.15	27.78	0.193	4.83	1.53	0.063	0.81	32.37	1.24	0.87	0.113
1260A-29R-3, 130–140	II	262.99	262.22	0.14	6.85	0.27	28.21	0.190	4.92	1.65	0.063	0.92	32.63	1.11	0.69	0.094
1260A-31R-4, 140–150	III	283.98	283.21	0.12	6.64	0.17	30.83	0.212	5.00	1.54	0.067	0.87	31.10	0.84	0.56	0.089
1260A-33R-3, 0–12	III	300.76	299.99	0.01	6.78	0.31	31.27	0.169	4.15	1.10	0.090	0.66	31.87	0.92	0.64	0.066
1260A-35R-1, 135–150	III	318.45	317.37	0.02	6.52	0.00	27.82	0.291	7.14	2.74	0.097	1.13	30.20	1.10	0.91	0.114
1260A-37R-3, 135–150	III	340.75	341.00	0.01	9.03	0.18	14.52	0.154	3.74	1.19	0.062	0.82	42.57	0.67	0.48	0.050
1260A-39R-4, 135–150	III	361.45	362.19	0.02	8.29	0.25	18.37	0.202	4.96	1.82	0.051	0.97	39.17	0.78	0.59	0.082
1260A-41R-1, 140–150	III	376.30	378.96	0.29	5.01	0.24	36.10	0.331	8.33	2.60	0.010	1.54	23.47	1.44	1.30	0.076
1260B-38R-5, 140–150	IV	451.36	455.43	0.80	10.25	2.85	5.24	0.080	1.48	0.87	0.000	0.78	47.80	0.35	0.24	0.440
1260B-40R-4, 140–150	IV	469.00	473.58	1.46	8.12	5.98	11.89	0.177	3.39	1.70	0.000	0.70	39.12	0.60	0.46	0.479
1260A-54R-2, 110–120	V	490.50	492.98	1.87	1.02	0.55	71.10	1.007	6.77	3.55	0.013	0.54	4.65	0.52	0.94	0.074
1260B-46R-3, 140–150	V	505.90	508.58	1.71	0.84	0.65	68.28	1.060	8.78	3.97	0.014	0.60	3.87	0.57	1.09	0.075
1261A-1R-2, 145–150	I	2.95	2.95	0.07	2.91	0.34	40.50	0.667	15.27	5.36	0.025	1.51	13.36	0.87	1.88	0.086
1261A-3R-1, 134–139	I	14.54	14.54	0.07	1.74	0.16	46.43	0.720	17.80	5.77	0.065	1.82	8.06	1.05	2.60	0.107
1261A-4R-1, 145–150	I	71.15	71.15	0.13	1.06	0.28	49.69	0.792	19.04	6.41	0.076	2.00	4.77	1.19	2.82	0.098
1261A-5R-4, 140–150	I	137.30	137.30	0.18	2.19	0.19	44.01	0.721	17.15	6.14	0.101	1.87	9.80	1.03	2.71	0.120
1261A-6R-5, 140–151	I	196.50	196.50	0.12	2.32	0.12	43.87	0.739	16.53	5.58	0.085	1.71	10.76	1.07	2.45	0.123
1261A-7R-3, 140–150	I	241.30	241.30	0.04	2.12	0.14	44.65	0.755	17.39	6.01	0.132	1.89	9.58	1.15	2.68	0.141
1261A-8R-3, 140–150	I	250.90	250.90	0.17	2.08	0.16	43.86	0.732	17.80	6.13	0.107	1.85	9.49	1.13	2.63	0.120
1261A-10R-3, 140–150	I	270.20	270.20	0.05	3.45	0.10	37.33	0.627	15.54	5.41	0.136	1.57	15.53	0.96	2.17	0.152
1261A-12R-5, 0–10	I	291.10	291.10	0.04	3.68	0.11	35.92	0.619	15.88	5.83	0.234	1.61	15.95	0.93	1.95	0.144
1261A-14R-6, 90–100	I	312.80	312.80	0.23	3.54	0.17	23.20	0.391	9.53	3.60	0.069	1.06	9.39	0.47	1.21	0.074
1261A-16R-3, 140–150	I	328.00	328.00	0.02	7.02	0.15	21.17	0.364	8.46	2.81	0.025	1.06	32.88	0.85	0.62	0.108
1261A-18R-5, 139–150	I	350.29	350.29	0.05	4.65	0.16	32.20	0.524	13.56	4.25	0.106	1.34	21.63	0.82	1.77	0.127
1261A-20R-6, 130–140	II	370.90	370.90	0.01	9.16	0.05	13.50	0.110	2.79	1.16	0.012	0.79	42.88	1.10	0.35	0.085
1261A-22R-3, 46–61	II	384.86	384.86	0.01	9.91	0.00	11.51	0.066	1.72	0.60	0.012	0.58	45.59	0.69	0.25	0.110
1261A-25R-4, 0 –7	II	414.64	414.64	0.01	9.51	0.04	14.28	0.061	1.59	0.57	0.018	0.58	44.81	0.68	0.22	0.083

Table AT2 (continued).

Hole, core, section, interval (cm)	Unit	Depth		Bulk parameter (wt%)			Major element oxide (wt%)									
		(mbsf)	(mcd)	TS	TIC	TOC	SiO$_2$	TiO$_2$	Al$_2$O$_3$	Fe$_2$O$_3$	MnO	MgO	CaO	Na$_2$O	K$_2$O	P$_2$O$_5$
1261A-28R-3, 138–150	II	442.98	442.98	0.01	8.88	0.00	19.53	0.072	1.80	0.66	0.027	0.58	41.30	0.80	0.30	0.069
1261A-32R-5, 140–150	II	484.60	484.60	0.02	7.18	0.05	26.87	0.196	4.91	1.68	0.049	0.88	33.62	1.06	0.71	0.104
1261A-35R-5, 0–15	III	512.10	512.10	0.19	4.79	0.19	37.51	0.361	8.73	3.37	0.059	1.36	22.55	1.44	1.06	0.184
1261A-37R-1, 135–150	III	526.65	526.65	0.06	7.10	0.03	25.06	0.230	5.85	2.07	0.065	0.94	33.46	1.23	0.78	0.231
1261A-39R-1, 135–150	III	545.95	545.95	0.23	8.20	0.20	18.37	0.189	4.70	1.39	0.029	0.99	38.56	0.96	0.66	0.089
1261A-45R-3, 136–152	IV	606.34	606.31	2.00	6.13	9.37	21.26	0.154	3.82	1.16	*0.000*	0.80	29.59	1.31	0.61	0.548
1261B-11R-2, 147–157	IV	619.37	612.38	2.46	5.81	10.89	22.32	0.159	3.91	1.34	*0.000*	0.81	27.51	1.22	0.57	0.076
1261A-48R-5, 136–150	IV	638.31	635.37	3.26	4.42	11.98	30.24	0.188	4.49	2.19	*0.000*	0.67	21.57	1.48	0.71	0.348
1261B-14R-2, 130–140	IV	648.00	647.25	2.22	6.39	9.21	16.24	0.195	4.38	1.78	*0.000*	1.04	32.42	1.05	0.66	1.570

Notes: Italics = below detection limit. TS = total sulfur, TIC = total inorganic carbon, TOC = total organic carbon.

Table AT3. Trace element concentrations in sediments of Demerara Rise using pore water squeezing residues. (**See table note.** Continued on next three pages.)

Hole, core, section, interval (cm)	Unit	Depth (mbsf)	(mcd)	As	Ba	Co	Cr	Cu	Mo	Ni	Pb	Rb	Sr	U	V	Y	Zn	Zr
207-																		
1257A-1H-1, 145–150	I	1.45	1.45	5	298	9	71	24	1	27	19	129	345	3	131	18	101	105
1257A-2H-4, 145–150	II	8.55	8.55	2	577	5	28	17	0	22	2	28	1,152	2	37	11	28	39
1257A-3H-4, 145–150	II	18.05	18.05	3	366	3	20	12	0	13	2	19	1,028	1	25	10	31	32
1257A-4H-3, 145–150	II	26.05	26.05	3	377	5	17	22	0	16	1	21	1,083	0	28	11	33	29
1257A-5H-3, 145–150	II	35.55	35.55	2	523	7	30	27	0	23	5	30	1,057	1	78	12	45	51
1257A-6X-3, 145–150	II	45.05	45.05	1	466	1	11	6	0	2	0	8	872	1	15	6	28	15
1257A-7X-3, 145–150	II	49.35	49.35	1	405	2	14	7	0	4	0	10	826	2	12	6	16	14
1257B-3R-2, 145–150	II	52.75	56.12	1	499	2	14	13	0	8	1	14	974	0	18	10	26	23
1257A-8X-3, 145–150	II	58.55	58.55	1	740	2	13	16	0	5	0	11	720	2	18	7	23	17
1257B-4R-3, 143–150	II	63.82	70.93	1	1,617	5	19	17	0	17	6	21	696	2	60	11	36	29
1257B-5R-4, 42–49	II	73.65	76.70	1	1,165	4	27	13	0	18	4	27	862	1	55	12	49	36
1257B-7R-2, 143–150	III	91.23	95.60	1	1,084	4	34	15	0	21	5	25	956	3	56	12	43	40
1257B-8R-4, 142–150	III	103.79	107.22	1	782	5	30	21	0	15	9	36	960	3	66	12	33	45
1257B-9R-3, 140–150	III	112.02	113.79	2	717	5	37	14	0	15	3	37	1,048	2	71	14	46	50
1257A-14X-4, 140–150	III	117.70	117.70	2	1,037	6	39	13	0	29	5	43	1,012	2	65	13	59	53
1257B-10R-4, 140–150	III	123.10	125.68	1	822	4	39	13	0	19	5	43	1,022	1	79	13	53	53
1257A-15X-5, 140–150	III	128.90	128.49	1	870	7	44	15	0	25	11	44	1,036	2	88	12	67	56
1257B-11R-4, 140–150	III	132.70	135.28	2	960	9	56	27	0	37	8	60	804	1	104	15	91	67
1257B-12R-3, 140–150	III	140.60	143.27	1	863	6	45	30	0	33	8	47	964	1	77	16	69	59
1257B-13R-4, 140–150	III	151.70	154.90	1	969	5	35	17	0	18	3	39	889	3	35	13	42	51
1257C-8R-6, 90–100	III	157.50	159.95	1	2,084	5	30	17	0	10	3	34	974	2	26	12	69	43
1257A-18X-4, 140–150	III	156.16	161.96	3	1,413	10	49	43	0	32	7	53	862	2	48	15	68	66
1257C-9R-6, 51–61	III	166.15	168.56	1	294	4	35	23	0	11	4	33	670	3	30	17	25	50
1257C-10R-1, 140–150	III	169.80	172.21	2	535	5	65	23	0	17	8	59	712	2	55	24	61	99
1257C-12R-2, 90–100	IV	190.10	192.65	33	223	0	318	29	52	59	2	80	741	27	1,075	45	494	32
1257C-13R-2, 140–150	IV	200.20	202.75	14	341	3	104	48	40	90	1	18	789	11	1,015	16	1,152	23
1257C-15R-3, 17–27	IV	218.98	221.53	23	169	5	134	54	48	103	5	22	855	19	1,476	16	874	26
1257B-27R-3, 0–7	V	225.30	228.94	4	128	14	141	16	0	36	7	65	392	4	105	17	59	136
1257C-16R-6, 20–30	V	233.87	235.03	3	139	16	140	14	0	38	6	56	417	2	95	15	52	133
1257A-31X-1, 71–81	V	275.81	281.61	10	156	17	195	23	0	51	6	79	540	5	131	19	73	125
1258A-1R-1, 145–150	I	1.45	1.45	12	193	8	45	27	0	28	13	46	759	2	78	19	63	69
1258A-1R-2, 145–150	I	2.95	2.95	4	181	7	47	23	0	23	9	34	952	1	60	14	59	58
1258A-3R-4, 145–150	II	20.15	20.15	1	636	3	12	11	0	12	0	5	696	1	10	7	22	16
1258A-4R-4, 145–150	II	29.75	29.75	0	803	2	2	10	0	7	1	7	757	0	17	9	25	17
1258A-5R-3, 145–150	II	37.65	42.15	3	745	5	22	38	0	22	5	26	722	2	41	12	46	41
1258A-6R-4, 145–150	II	48.75	49.27	2	1,068	11	34	29	1	38	8	42	548	3	60	14	71	65
1258A-7R-4, 145–150	II	58.15	59.14	3	1,081	9	36	54	0	34	8	37	591	2	61	14	61	56
1258A-8R-4, 140–150	II	68.07	69.92	2	1,123	4	24	21	0	17	7	28	654	2	78	15	40	46
1258A-9R-6, 140–150	II	80.80	81.05	2	1,306	4	51	19	0	34	10	33	549	0	44	18	47	57
1258A-10R-3, 140–150	II	86.00	86.63	2	1,159	7	36	28	0	28	8	35	643	1	84	17	58	58
1258A-11R-5, 135–145	II	98.65	98.35	2	1,478	8	45	35	0	31	10	45	612	3	77	16	73	68
1258A-12R-5, 140–150	II	108.30	108.69	1	1,259	5	37	21	1	23	10	40	645	3	59	17	52	63
1258A-13R-4, 140–150	II	116.40	117.01	2	1,289	6	35	25	0	23	7	32	710	3	66	15	55	51
1258B-14R-4, 140–150	II	133.80	134.22	2	950	4	31	24	0	14	6	26	658	3	46	15	41	42
1258B-18R-3, 140–150	II	170.90	171.49	2	961	5	24	49	0	16	4	21	733	0	45	11	34	35
1258A-17R-4, 140–150	II	154.95	176.79	3	1,061	3	36	21	0	18	3	26	720	1	63	12	44	40

Table AT3 (continued).

Hole, core, section, interval (cm)	Unit	Depth (mbsf)	Depth (mcd)	As	Ba	Co	Cr	Cu	Mo	Ni	Pb	Rb	Sr	U	V	Y	Zn	Zr
1258A-20R-2, 140–150	II	181.00	204.43	1	1,117	5	30	10	0	16	4	27	858	0	57	11	44	43
1258A-22R-3, 140–150	II	201.50	224.93	1	768	5	30	20	0	18	4	31	934	2	65	12	47	46
1258A-24R-3, 139–150	II	220.69	244.12	1	641	6	37	18	0	19	8	33	870	1	70	14	47	49
1258A-26R-2, 140–150	II	238.50	260.95	2	866	11	53	24	0	47	10	48	777	2	123	17	87	67
1258A-28R-5, 145–150	II	262.35	284.80	1	289	7	24	20	0	16	2	26	793	1	32	9	30	32
1258A-30R-2, 140–150	II	277.10	299.47	1	410	4	32	19	0	20	5	37	866	5	35	11	41	49
1258A-32R-5, 140–150	II	300.90	324.11	1	1,580	2	27	29	0	16	3	33	613	1	32	12	34	39
1258B-33R-4, 140–150	II	307.00	329.81	1	168	6	48	25	0	33	6	59	715	3	51	15	59	67
1258B-36R-3, 90–100	III	334.00	346.81	2	148	5	42	11	0	14	3	44	653	2	37	15	31	55
1258A-35R-3, 140–150	III	326.80	349.67	1	11,018	7	323	17	38	193	5	34	855	1	32	15	33	48
1258A-37R-2, 145–150	III	344.65	367.52	1	125	4	38	17	0	15	1	34	621	2	25	16	29	47
1258A-39R-1, 63–73	III	361.53	382.27	1	215	5	53	19	0	22	5	51	689	1	45	17	49	70
1258B-39R-5, 135–150	III	366.35	384.10	1	659	7	56	26	0	22	6	55	713	4	46	18	45	67
1258B-43R-2, 110–120	III	390.40	412.51	1	165	5	43	26	1	19	4	39	424	2	33	16	52	45
1258B-45R-2, 75–85	IV	399.25	420.08	24	477	8	127	93	149	211	9	37	768	16	2,111	13	1,964	38
1258B-46R-1, 31–44	IV	403.41	425.47	31	701	15	78	84	23	108	3	29	769	7	319	14	99	36
1258B-51R-2, 20–29	IV	427.92	452.24	25	595	5	159	77	104	147	7	36	726	44	2,039	22	705	38
1258B-52R-2, 70–80	IV	433.71	458.03	20	463	4	192	65	83	144	4	27	828	17	1,778	16	532	35
1258B-54R-3, 0–10	IV	444.38	468.86	20	207	6	174	49	73	127	6	40	705	22	1,584	22	405	78
1258B-55R-3, 58–68	IV	448.27	475.13	43	270	12	184	48	117	272	7	65	392	47	973	29	715	170
1258C-30R-1, 112–122	V	462.52	495.02	23	249	13	209	53	26	116	11	90	282	7	1,101	13	608	101
1258C-34R-2, 135–150	V	483.55	516.05	7	247	16	186	37	0	60	11	88	341	2	169	17	151	130
1259A-1R-2, 105–110	I	2.55	2.55	1	211	2	14	8	0	9	4	11	1,108	0	12	9	23	23
1259A-2R-2, 145–150	I	11.75	11.75	1	218	3	15	22	0	12	1	11	890	1	19	10	26	26
1259A-3R-4, 145–150	I	24.25	24.25	1	343	2	16	12	0	8	1	13	1,110	3	17	9	22	28
1259A-5R-2, 145–150	II	39.35	39.35	0	177	3	15	20	0	12	1	10	920	1	0	9	19	18
1259A-6R-2, 145–150	II	48.45	48.45	1	183	2	17	10	0	11	0	12	1,052	3	28	9	23	22
1259A-7R-4, 145–150	II	60.55	60.55	0	256	2	14	17	0	10	4	14	1,071	2	6	9	22	23
1259A-8R-4, 145–150	II	69.75	69.75	1	251	2	19	28	0	11	4	15	1,248	2	20	8	19	26
1259A-9R-5, 145–150	II	80.35	80.35	1	369	6	21	11	0	13	3	21	1,213	3	38	9	41	30
1259A-10R-5, 140–150	II	90.00	90.00	1	228	3	22	10	0	12	3	18	1,268	3	33	9	30	30
1259A-12R-5, 140–150	II	109.40	109.40	1	216	2	13	17	0	6	1	11	1,128	2	17	8	22	19
1259A-14R-3, 140–150	II	125.70	125.70	1	315	4	18	10	0	17	4	15	1,078	0	26	14	31	37
1259A-16R-1, 140–150	II	142.00	142.00	1	245	1	17	6	0	7	1	10	846	1	15	6	16	18
1259A-18R-1, 135–145	II	161.15	161.15	1	366	3	14	6	0	7	0	10	864	1	17	7	13	18
1259A-20R-4, 130–140	II	185.00	185.00	1	459	2	8	13	0	4	1	7	818	1	14	6	58	16
1259A-22R-3, 140–150	II	202.90	202.90	1	472	2	10	12	0	10	1	9	893	0	12	8	18	18
1259A-24R-1, 132–142	II	219.12	219.12	1	361	0	8	7	0	4	0	8	634	2	5	8	14	13
1259A-26R-5, 140–150	II	244.30	244.30	1	369	1	7	5	0	2	0	4	713	2	3	7	14	11
1259A-29R-4, 140–150	II	271.70	271.70	1	715	4	11	8	0	12	2	7	708	1	13	8	19	19
1259A-32R-1, 133–143	II	296.03	296.03	0	677	3	16	12	0	17	7	19	784	2	25	15	38	38
1259A-34R-2, 140–150	II	316.92	316.77	2	1,333	5	30	13	0	26	4	32	837	2	52	16	54	54
1259A-36R-1, 140–150	II	334.70	335.30	1	911	5	26	18	0	20	3	21	772	2	40	10	48	33
1259A-38R-1, 140–150	II	354.00	354.83	2	1,115	7	29	13	0	28	3	26	839	1	47	11	52	40
1259A-40R-3, 90–100	III	375.70	374.85	9	1,036	19	28	28	0	47	2	24	942	3	51	11	50	42
1259A-43R-1, 140–150	III	402.10	403.27	1	1,018	21	40	28	0	52	4	40	1,005	1	77	13	48	54
1259A-45R-2, 140–150	III	422.90	424.38	1	857	7	39	17	0	29	4	33	964	1	49	17	58	50
1259A-48R-3, 138–150	III	453.18	453.19	1	357	4	18	14	0	13	1	21	803	2	21	9	25	29
1259A-50R-5, 137–149	III	475.06	475.59	1	5,268	6	26	16	0	20	3	38	807	1	34	13	34	50

Table AT3 (continued).

Hole, core, section, interval (cm)	Unit	Depth (mbsf)	Depth (mcd)	As	Ba	Co	Cr	Cu	Mo	Ni	Pb	Rb	Sr	U	V	Y	Zn	Zr
1259A-52R-1, 103–117	III	488.33	490.08	1	168	0	34	20	0	11	2	34	676	4	34	14	45	49
1259C-16R-5, 137–150	IV	525.65	529.18	14	597	5	104	46	38	87	2	21	813	10	572	13	584	28
1259C-17R-1, 136–146	IV	529.26	532.38	19	832	3	58	34	87	155	3	21	924	11	942	6	294	23
1259C-18R-4, 140–150	IV	543.40	547.73	23	945	11	59	60	19	175	3	24	770	18	232	16	60	28
1259C-19R-2, 78–88	V	549.22	551.57	5	219	21	127	41	2	35	10	105	96	4	127	22	51	256
1259B-25R-1, 89–100	V	554.09	555.18	5	187	12	98	29	0	22	6	82	135	4	107	22	65	306
1260A-1R-1, 58–63	I	0.58	0.58	9	595	15	75	36	1	31	27	124	311	5	165	24	107	131
1260A-2R-1, 145–150	II	2.45	2.45	4	126	4	35	10	0	17	8	33	985	2	50	8	36	51
1260A-3R-1, 145–150	II	11.75	11.75	1	372	5	26	12	0	14	3	23	1,129	3	37	13	33	43
1260A-4R-3, 145–150	II	23.95	23.95	2	281	2	25	14	0	15	2	24	1,294	3	51	8	21	36
1260A-6R-5, 90–100	II	45.10	45.10	1	319	1	13	21	0	4	0	11	754	2	14	8	21	22
1260A-7R-5, 145–150	II	54.95	55.05	1	419	4	9	20	0	10	2	10	819	0	10	7	14	14
1260A-8R-5, 142–150	II	64.62	64.72	0	356	1	8	7	0	5	0	5	909	2	7	8	12	15
1260A-9R-5, 142–150	II	74.32	73.32	1	683	0	9	10	0	6	0	11	898	3	10	8	16	17
1260A-10R-5, 142–150	II	84.02	83.12	9	342	5	8	21	0	17	0	6	790	1	12	9	23	16
1260A-12R-4, 140–150	II	101.80	100.42	1	585	2	12	7	0	5	0	4	706	0	0	8	21	13
1260A-14R-6, 105–110	II	123.85	122.17	1	396	4	12	5	0	7	1	8	577	1	14	10	14	19
1260A-17R-1, 145–150	II	145.65	143.84	1	451	2	11	9	0	6	0	10	684	3	12	7	13	17
1260A-19R-5, 143–150	II	170.63	168.82	2	734	2	16	14	0	9	0	10	703	1	16	8	20	21
1260A-21R-1, 130–140	II	183.80	181.99	1	624	5	15	13	0	10	0	11	603	1	15	8	18	20
1260A-23R-2, 140–150	II	204.30	202.49	1	621	3	16	13	0	17	4	16	728	2	21	14	34	33
1260A-25R-2, 141–150	II	223.61	221.80	1	843	5	69	17	0	31	8	29	713	2	43	15	50	53
1260A-27R-4, 140–150	II	245.90	244.39	4	639	7	26	21	0	24	1	24	764	2	45	14	50	43
1260A-29R-3, 130–140	II	262.99	262.22	1	800	4	28	16	0	16	5	24	759	3	50	10	40	39
1260A-31R-4, 140–150	III	283.98	283.21	2	1,288	3	27	14	0	17	3	28	808	2	50	14	38	45
1260A-33R-3, 0–12	III	300.76	299.99	2	93	1	26	52	0	4	1	21	889	2	39	11	18	37
1260A-35R-1, 135–150	III	318.45	317.37	1	2,118	6	50	17	0	34	9	37	888	2	68	15	64	54
1260A-37R-3, 135–150	III	340.75	341.00	2	1,479	3	19	21	0	12	1	23	804	3	26	9	24	31
1260A-39R-4, 135–150	III	361.45	362.19	1	123	3	26	12	2	17	2	29	695	1	33	13	66	41
1260A-41R-1, 140–150	III	376.30	378.96	3	82	6	53	17	0	25	5	59	919	2	41	14	54	71
1260B-38R-5, 140–150	IV	451.36	455.43	19	85	2	72	27	100	195	3	12	918	36	1,081	13	743	18
1260B-40R-4, 140–150	IV	469.00	473.58	35	144	4	149	43	132	216	3	24	989	34	1,758	16	798	44
1260A-54R-2, 110–120	V	490.50	492.98	8	200	8	148	14	1	20	4	51	211	3	81	20	32	457
1260B-46R-3, 140–150	V	505.90	508.58	9	209	14	358	15	28	152	8	60	183	3	105	22	39	375
1261A-1R-2, 145–150	I	2.95	2.95	5	459	12	66	29	0	28	22	101	535	4	137	25	89	117
1261A-3R-1, 134–139	I	14.54	14.54	7	394	14	66	23	0	29	21	137	374	3	144	22	101	120
1261A-4R-1, 145–150	I	71.15	71.15	8	371	14	75	23	1	32	24	146	269	2	154	24	107	131
1261A-5R-4, 140–150	I	137.30	137.30	12	383	14	73	18	0	33	22	143	454	2	134	24	96	126
1261A-6R-5, 140–151	I	196.50	196.50	17	366	16	70	18	0	32	22	131	504	2	138	23	92	135
1261A-7R-3, 140–150	I	241.30	241.30	12	404	15	71	19	0	30	24	143	484	3	143	25	95	131
1261A-8R-3, 140–150	I	250.90	250.90	14	396	17	72	22	0	36	26	146	515	4	141	24	96	120
1261A-10R-3, 140–150	I	270.20	270.20	12	343	12	72	17	0	28	18	121	722	3	129	20	85	104
1261A-12R-5, 0–10	I	291.10	291.10	9	302	10	67	22	0	25	19	114	738	3	122	18	84	98
1261A-14R-6, 90–100	I	312.80	312.80	8	191	8	40	4	1	17	8	65	350	2	78	12	48	58
1261A-16R-3, 140–150	I	328.00	328.00	2	421	7	48	19	0	18	13	33	1,120	2	57	15	55	72
1261A-18R-5, 139–150	I	350.29	350.29	6	316	11	61	20	0	26	17	95	872	2	106	18	67	85
1261A-20R-6, 130–140	II	370.90	370.90	0	491	3	19	9	0	7	2	14	951	4	17	8	18	28
1261A-22R-3, 46–61	II	384.86	384.86	0	449	2	11	8	0	4	2	9	871	2	12	8	15	19
1261A-25R-4, 0 –7	II	414.64	414.64	0	503	2	8	8	0	9	0	7	625	0	9	7	16	17

Table AT3 (continued).

Hole, core, section, interval (cm)	Unit	Depth (mbsf)	Depth (mcd)	As	Ba	Co	Cr	Cu	Mo	Ni	Pb	Rb	Sr	U	V	Y	Zn	Zr
										Trace element (ppm)								
1261A-28R-3, 138–150	II	442.98	442.98	*1*	962	*2*	*11*	14	*0*	*6*	2	9	793	*1*	*11*	9	20	19
1261A-32R-5, 140–150	II	484.60	484.60	*1*	1,118	5	*29*	20	*0*	20	3	25	860	*1*	41	12	51	41
1261A-35R-5, 0 –15	III	512.10	512.10	*1*	1,158	7	44	30	*0*	34	8	47	901	3	80	23	94	72
1261A-37R-1, 135–150	III	526.65	526.65	*1*	1,387	19	30	17	*0*	58	6	29	987	*1*	42	22	49	48
1261A-39R-1, 135–150	III	545.95	545.95	*1*	3,776	5	31	18	*0*	*15*	4	28	871	*1*	26	10	26	41
1261A-45R-3, 136–152	IV	606.34	606.31	16	896	*2*	137	53	136	136	5	22	1,047	15	1,655	12	1,037	28
1261B-11R-2, 147–157	IV	619.37	612.38	28	912	3	90	48	147	227	4	23	964	11	1,355	*4*	937	27
1261A-48R-5, 136–150	IV	638.31	635.37	28	1,178	9	51	51	55	190	4	25	897	18	559	19	165	35
1261B-14R-2, 130–140	IV	648.00	647.25	36	400	5	150	74	78	141	6	29	876	24	2,054	15	1,404	34

Note: Italics = below detection limit.

A. Hetzel et al.
Inorganic Geochemical Characterization of Lithologic Units

36

Table AT4. Rare earth element concentrations in sediments of Demerara Rise (Site 1258) using pore water squeezing residues.

Hole, core, section, interval (cm)	Unit	Depth (mbsf)	Depth (mcd)	La	Ce	Pr	Nd	Sm	Eu	Gd	Tb	Dy	Ho	Er	Tm	Yb	Lu
207-																	
1258A-1R-1, 145–150	I	1.45	1.45	24.63	45.35	5.86	21.34	4.18	0.92	3.90	0.57	3.20	0.63	1.76	0.24	1.60	0.24
1258A-1R-2, 145–150	I	2.95	2.95	19.46	37.48	4.62	16.54	3.15	0.66	2.71	0.40	2.29	0.45	1.28	0.16	1.24	0.16
1258A-3R-4, 145–150	II	20.15	20.15	7.28	7.87	1.53	5.94	1.18	0.31	1.22	0.19	1.04	0.21	0.56	0.06	0.55	0.07
1258A-4R-4, 145–150	II	29.75	29.75	8.31	10.40	1.76	7.28	1.43	0.36	1.36	0.21	1.22	0.25	0.67	0.07	0.71	0.09
1258A-5R-3, 145–150	II	37.65	42.15	16.26	25.97	3.61	13.33	2.64	0.61	2.56	0.38	2.15	0.44	1.22	0.17	1.19	0.17
1258A-6R-4, 145–150	II	48.75	49.27	19.58	37.08	4.44	15.83	3.02	0.66	2.75	0.42	2.39	0.48	1.33	0.18	1.29	0.18
1258A-7R-4, 145–150	II	58.15	59.14	20.23	38.82	4.55	16.45	3.07	0.69	2.82	0.44	2.44	0.49	1.36	0.18	1.33	0.18
1258A-8R-4, 140–150	II	68.07	69.92	17.70	32.18	3.93	14.66	2.79	0.61	2.57	0.39	2.30	0.46	1.28	0.17	1.21	0.17
1258A-9R-6, 140–150	II	80.80	81.05	21.43	43.23	5.06	17.71	3.39	0.77	3.29	0.49	2.80	0.56	1.52	0.21	1.50	0.22
1258A-10R-3, 140–150	II	86.00	86.63	20.82	41.10	4.81	17.97	3.36	0.72	3.12	0.47	2.74	0.56	1.63	0.21	1.59	0.22
1258A-11R-5, 135–145	II	98.65	98.35	24.50	50.31	5.58	20.23	3.72	0.82	3.38	0.50	2.98	0.58	1.64	0.22	1.56	0.23
1258A-12R-5, 140–150	II	108.30	108.69	21.58	43.68	4.91	17.85	3.35	0.74	3.20	0.48	2.76	0.54	1.55	0.21	1.48	0.21
1258A-13R-4, 140–150	II	116.40	117.01	18.57	35.46	4.26	15.19	2.96	0.67	2.74	0.41	2.31	0.47	1.27	0.17	1.23	0.17
1258B-14R-4, 140–150	II	133.80	134.22	15.59	27.49	3.37	12.56	2.42	0.53	2.23	0.35	1.93	0.41	1.16	0.15	1.10	0.15
1258B-18R-3, 140–150	II	170.90	171.49	14.40	25.99	3.21	12.11	2.21	0.49	2.05	0.30	1.73	0.35	0.95	0.12	0.94	0.13
1258B-17R-4, 140–150	II	154.95	176.79	12.53	21.28	2.74	10.15	1.98	0.45	1.88	0.27	1.55	0.32	0.85	0.11	0.83	0.11
1258B-20R-2, 140–150	II	181.00	204.43	12.33	22.07	2.76	10.86	2.16	0.48	1.98	0.30	1.79	0.37	1.05	0.12	1.08	0.14
1258B-22R-3, 140–150	II	201.50	224.93	14.67	26.77	3.37	12.16	2.31	0.52	2.21	0.33	1.90	0.40	1.07	0.15	1.09	0.15
1258B-24R-3, 139–150	II	220.69	244.12	16.14	29.98	3.57	13.42	2.57	0.57	2.37	0.37	2.16	0.45	1.23	0.17	1.25	0.18
1258B-26R-2, 140–150	II	238.50	260.95	24.97	46.44	6.28	22.37	4.32	0.97	4.03	0.59	3.25	0.64	1.74	0.23	1.60	0.23
1258B-28R-5, 145–150	II	262.35	284.80	13.09	23.05	2.80	10.35	1.99	0.44	1.81	0.27	1.55	0.31	0.84	0.11	0.84	0.12
1258B-30R-2, 140–150	II	277.10	299.47	17.14	30.76	3.88	14.10	2.55	0.57	2.34	0.34	1.97	0.39	1.05	0.14	1.00	0.13
1258B-32R-5, 140–150	II	300.90	324.11	15.86	29.79	3.53	12.35	2.32	0.51	2.08	0.33	1.92	0.39	1.04	0.14	1.06	0.15
1258B-33R-4, 140–150	II	307.00	329.81	22.90	45.20	5.35	19.33	3.52	0.76	3.09	0.46	2.57	0.51	1.38	0.19	1.30	0.19
1258B-36R-3, 90–100	III	334.00	346.81	18.46	32.35	3.94	14.84	2.73	0.58	2.48	0.38	2.17	0.46	1.29	0.18	1.32	0.20
1258A-35R-3, 140–150	III	326.80	349.67	16.73	29.39	3.53	12.60	2.39	0.43	2.16	0.34	1.97	0.41	1.14	0.15	1.12	0.17
1258A-37R-2, 145–150	III	344.65	367.52	17.56	30.22	3.69	13.27	2.35	0.54	2.32	0.36	2.13	0.46	1.31	0.18	1.31	0.19
1258A-39R-1, 63–73	III	361.53	382.27	20.10	34.78	4.51	16.24	3.14	0.67	2.86	0.44	2.61	0.55	1.65	0.21	1.61	0.22
1258B-39R-5, 135–150	III	366.35	384.10	21.36	37.30	4.66	16.49	3.06	0.68	2.82	0.44	2.55	0.53	1.55	0.21	1.43	0.21
1258B-43R-2, 110–120	III	390.40	412.51	18.47	30.07	3.91	15.25	2.80	0.62	2.62	0.39	2.30	0.49	1.48	0.18	1.39	0.19
1258B-45R-2, 75–85	IV	399.25	420.08	12.60	18.81	2.68	10.11	1.99	0.48	1.86	0.27	1.53	0.32	0.86	0.10	0.78	0.11
1258B-46R-1, 31–44	IV	403.41	425.47	11.11	18.02	2.89	10.81	2.43	0.64	2.47	0.38	2.21	0.44	1.17	0.15	1.05	0.14
1258B-51R-2, 20–29	IV	427.92	452.24	16.52	23.70	3.28	12.69	2.54	0.61	2.62	0.40	2.52	0.56	1.71	0.21	1.66	0.23
1258B-52R-2, 70–80	IV	433.71	458.03	13.26	19.50	2.70	10.20	2.03	0.50	1.96	0.30	1.79	0.40	1.14	0.15	1.14	0.17
1258B-54R-3, 0–10	IV	444.38	468.86	19.53	34.37	4.58	15.96	3.12	0.73	2.98	0.48	2.90	0.62	1.85	0.25	1.88	0.26
1258B-55R-3, 58–68	IV	448.27	475.13	30.68	57.54	6.86	25.52	4.96	1.18	4.79	0.77	4.58	0.96	2.82	0.40	2.70	0.41
1258C-30R-1, 112–122	V	462.52	495.02	19.24	40.08	4.95	17.46	3.58	0.83	2.98	0.45	2.46	0.48	1.36	0.18	1.34	0.19
1258C-34R-2, 135–150	V	483.55	516.05	29.74	56.82	6.65	23.21	4.30	0.97	3.71	0.56	3.25	0.65	1.86	0.27	1.88	0.28